The role of the solvent in the reactivity of bis-4-imidazoline-2-selone derivatives towards I_2: an experimental and theoretical approach

M. Carla Aragoni, Massimiliano Arca, Claudia Caltagirone, Carlo Castellano, Francesco Demartin, Peter G. Jones, Tiziana Pivetta, Enrico Podda, Vito Lippolis,* Sergio Murgia, Giacomo Picci

ABSTRACT: The reactivity of 1,1'-bis(3-methyl-4-imidazolin-2-selone)methane (**L1**) and 1,2-bis(3-methyl-4-imidazolin-2-selone)ethane (**L2**) towards I_2 has been explored in MeCN under different experimental conditions and compared with that in CH_2Cl_2. The compounds [**L1'**]$(I)_2$ (**I**), [**L1**I]$_n(I)_n$ (**II**), [**L1**(μ-Se)]$(I)_2\cdot½H_2O$ (**III**), [**L1**I]$(I_3)\cdot 2I_2$ (**IV**) and [**L2**]$(I)_2\cdot$MeCN (**V**) were obtained and characterized. X-ray diffraction analyses point out an ionic nature for these compounds, which is presumably favored by the polarity of the solvent used. In particular, [**L1**I]$_n(I)_n$ (**II**) represents the first example of an iodonium complex of imidazoline-2-selone derivatives, while [**L1**(μ-Se)]$(I)_2\cdot½H_2O$ (**III**) represents a unique example of a dicationic [RSeSeSeR] triselane. DFT calculations have allowed to better understand the nature of the obtained compounds and to justify their formations in polarizing reaction conditions rather than in low polar solvents.

INTRODUCTION

Over the past two decades, thio- and seleno-amide compounds, in particular imidazoline-2-chalcogenone derivatives such as 1-methyl-2-mercaptoimidazole (MMI) and its Se-analogue (MSeI), have received great attention because of to their potential biological applications, both as anti-thyroid drugs in the treatment of hyperthyroidism[1-4] and as potential anti-oxidants for preventing metal-mediated oxidative damage of DNA.[5-8]

The need to understand the mechanism of the anti-thyroid drug activity and to identify the species produced in the interaction with the thyroid peroxidase (TPO)/H_2O_2/I^- enzymatic system within the thyroid gland,[2, 3, 9-12] has stimulated many chemists to study the reactivity of these compounds and structural analogues towards di-halogens (I_2, Br_2), inter-halogens (IBr, ICl), and *pseudo*-halogens or di-halogen like electrophilic compounds (ICN, MesTeI [Mes = 2,4,6-$(CH_3)_3C_6H_2$]) both in solution and in the solid state.[3, 13-15]

Solution studies in low polar solvents (mainly CH_2Cl_2) on the interaction between chalcogen donor molecules and I_2 to form 1:1 I_2 charge-transfer (CT) "spoke" adducts indicate that Se-donors bind I_2 more strongly than the corresponding S-isologues, and that thiones and selones are stronger donors than sulphides and selenides.[16] Importantly, the formation constants of 1:1 I_2 CT adducts have been proved to strongly depend on the chemical environment of the chalcogen donor atom and vary over a wide range as a consequence of subtle variations in the chemical structure of the donor molecule. As an example, solution studies performed on the representative pentatomic heterocyclic thio- and seleno-amides donors shown in Scheme 1, showed that the presence of two nitrogen atoms in the five-membered ring increases the donor ability of the chalcogenone group, as compared to related compounds containing only one nitrogen atom.

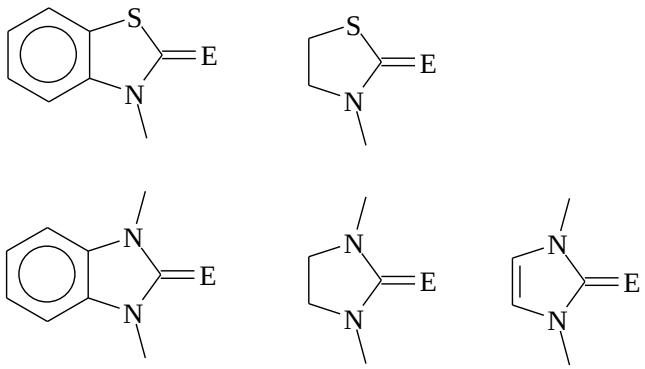

Scheme 1. Representative five-membered heterocyclic thio- and seleno-amides donors: E = S, Se.

An increase in the formation constant (K_f) of the corresponding 1:1 I_2 CT adducts, was also observed on going from benzoimidazole systems to imidazolidine analogues, and finally to imidazoline-2-chalcogenone derivatives, thus defining a scale of donor strength towards I_2 within this class of

chalcogen donor molecules and explaining the "I_2 sponge" action of the anti-thyroid drug MMI in the thyroid gland (Scheme 2).

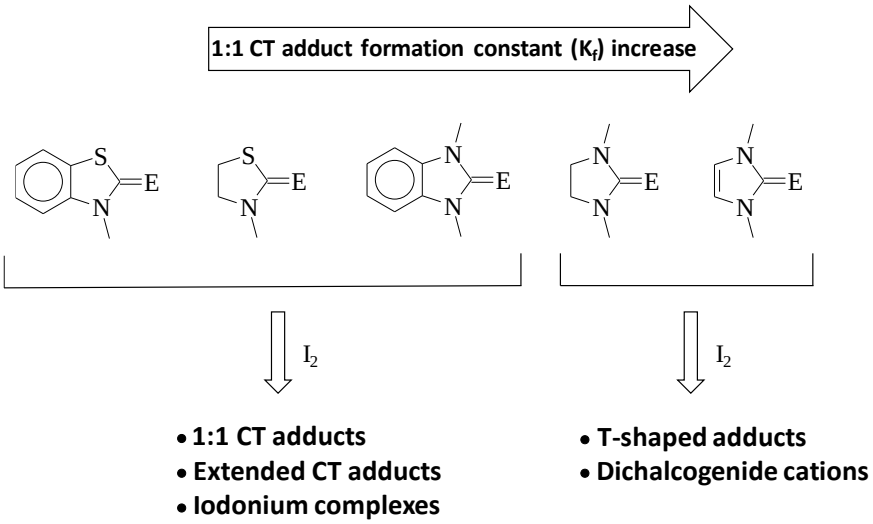

Scheme 2. Prevailing products in the solid state from the reaction of I_2 with representative five-membered heterocyclic thio- and seleno-amides RE donors: R = organic framework; E = S, Se.

The nature of the products obtainable in the solid state strongly depends on the identity of the chalcogen atom (S or Se), its chemical surroundings, the acid/base/redox properties of the reactants, and the experimental conditions used.[17] The wide variety of products characterized since now makes it difficult to establish general rules for rationalizing the outcome of these reactions because many factors are involved and small variations either in the reaction conditions or in the structural features of the donor molecules can be crucial. Anyway, if one limits the discussion to the reactions between I_2 and diorganosulfur and selenium compounds R_2E (E = S, Se), the isolation of 1:1 CT adducts featuring an almost linear E–I–I moiety can be generally expected. On the contrary, a plethora of structurally different solid state products can be obtaining by reacting I_2 with thioamides and selenoamides, RE (E = S, Se), in particular those heterocyclic derivatives shown in Scheme 1.[17, 18] In particular, besides 1:1 CT adducts, the formation of "extended spoke" CT adducts RE–I_2–I_2 involving a second I_2 molecule interacting with the first one bound to the chalcogen atom, and iodonium salts, featuring a two-chalcogen-coordinated iodine(I) complexes $[RE–I–ER]^+$ (R = organic framework) is observed with the group of donors sketched on the left in Scheme 2.[19-22] In contrast, the prevailing

formation of I_2 "T-shaped" hypervalent adducts,[13c, 14b, 15] featuring an almost linear I–Se–I moiety, or diselenide cations, $[RSe–SeR]^{+n}$ (n = 1, 2), featuring a chalcogen-chalcogen bond[13, 23] is observed when molecules with a higher donor strength (higher 1:1 CT I_2-adducts formation constant in solution, K_f) are considered, especially Se-donor molecules and imidazoline derivatives, as shown on the right of Scheme 2. The formation of donor oxidation products is the rule, when Br_2[14c, 24-26] and inter-halogens (IBr, ICl) (in this latter case, especially with donors belonging to the group on the right in Scheme 2)[14a, 27-29] are employed because of their stronger oxidation properties.

Interestingly, no "T-shaped" I_2-adducts are known with S-donors, and the formation at the solid state of disulfide and diselenide cations from the direct reaction of I_2 with donors on the left-hand side of Scheme 2 has not been observed to date; the only examples known of diselenide dications for these donors were obtained from 1,3-dialkyl-1H-benzo[d]imidazole-2(3H)-selone derivatives by reaction of iron powder with their "T-shaped" di-halogen adducts (including a di-iodine "T-shaped" adduct, a rare example of this kind of adducts with non-imidazoline derivatives).[30] Furthermore, no iodonium complexes with imidazoline 2-chalcogenone derivatives have been isolated until now.

The difficulty to predict the nature of the final products is well emphasised by the case of the bis-4-imidazoline-2-selone derivatives **L1** and **L2** (Scheme 3), which differ in the length of the aliphatic bridge between the two five-membered rings. The reaction in CH_2Cl_2 of **L1** with I_2 affords the 1:2 CT I_2-adduct **1**; in contrast, the reaction of **L2** with I_2 in the same solvent and experimental conditions used for the reaction of **L1** affords the corresponding 1:2 "T-shaped" I_2-adduct **2**.[14b] For neither donors was the formation of diselenide cations observed from the direct reactions with I_2 (see below). The ionic compounds $[\mathbf{L2}]^{2+}\cdot 2I^-$ and $[\mathbf{L2}]^{2+}\cdot I_3^-\cdot ½I_4^-$ could only be obtained from the reaction of **2** (Scheme 3) with Tellurium (0) as powder in Et_2O.[14a] This result clearly shows the importance of subtle variations in the structure of the donor molecules in determining the outcome of the reactions with di-halogens and inter-halogens.

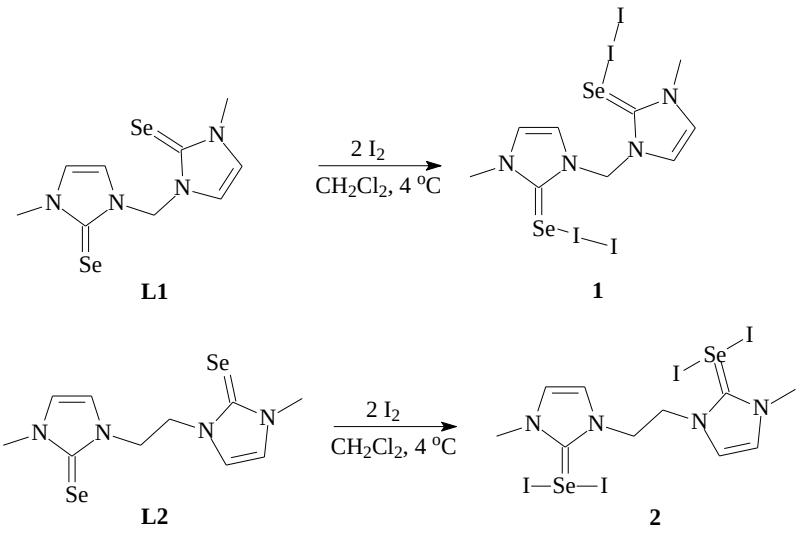

Scheme 3. Experimental conditions and products isolated at the solid state from the reaction of I_2 with bis-4-imidazoline-2-selone derivatives **L1** and **L2**.

Husebye and co-workers proposed a reaction scheme according to which the cations $[RE–X]^+$ (R = organic framework, E = S, Se, X = halogen) would represent the key intermediate in the formation of all final products obtained from the reactions between chalcogen donors and di-halogens and inter-halogens.[31] This cation might originate by heterolytic cleavage of the X–X or E–X bond from either the initially formed CT or "T-shaped" adducts, respectively. Although the formation of the $[RE–X]^+$ cation has not been directly proved yet, the natural charge distribution calculated for it at DFT level for different RE chalcogenone donors proved to be of great help in predicting and explaining the nature of the isolated final products.[25, 28] In particular, the highest tendency of imidazoline-2-selone derivatives among five-membered heterocyclic thio- and seleno-amides (Scheme 1) to afford "T-shaped" adducts and $[(RE)_2]^{2+}$ dications from the direct reaction with di-halogens (including I_2) and inter-halogens was predicted and experimentally verified, with only a few exceptions.

The possible key role played by the Husebye's $[RE–X]^+$ cations in the reaction of chalcogenone donors with di-halogens and inter-halogens, together with the results reported for the reactions of **L1** and **L2** with I_2 (Scheme 3), suggests an active role of the solvent in determining the nature of the final outcome of these reactions: polar solvents are expected to stabilize ionic products, whilst low-polar solvents neutral ones. We report here a systematic exploration of the reactions between **L1** and **L2**

with I_2 performed in MeCN under different experimental conditions, with the aim of promoting the formation of ionic compounds such as iodonium complexes and diselenide dications from the direct reaction of these donors with I_2.

RESULTS AND DISCUSSION

Synthesis and characterization

The reaction between L1 and I_2 in 1:1 molar ratio was performed in air in MeCN at room temperature (24h stirring). Upon slow evaporation of the resulting orange solution, we were able to isolate a few crystals from the amorphous mass thus formed. These displayed three different morphologies, shapes and colours. X-ray diffraction analysis allowed establishing the nature of the corresponding compounds [**L1**'](I)$_2$ (**I**), ([**L1**I]$_n$(I)$_n$ (**II**) and ([**L1**(μ-Se)](I)$_2$·½H_2O (**III**), detailed in Scheme 4 (see below for the description of the structures).

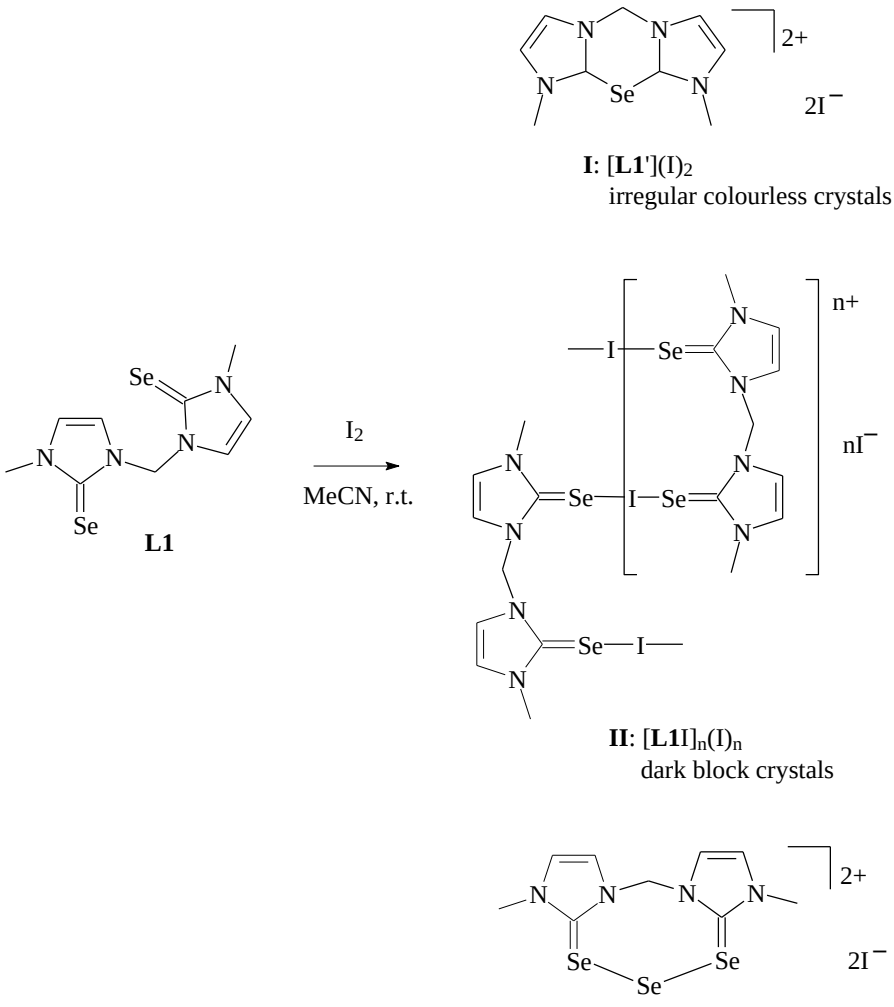

Scheme 4. Molecular schemes of the ionic compounds **I**, **II**, and **III** isolated as single crystals from the reaction of **L1** with I_2 (1:1 molar ratio) in MeCN as established by X-ray diffraction analysis.

The reaction was repeated in the presence of one equiv. of Se powder under the same experimental conditions, but for a longer reaction time (72h stirring at room temperature). A yellowish solid and an orange solution were present in the reaction mixture, which were separated by filtration. Dark red blocks of (**II**) formed by slow evaporation of the solution at room temperature in air (7.1% yield) as confirmed by elemental and X-ray analysis. ESI-MS spectrum in positive ion mode exhibited peaks at *m/z*: 463, 336 and 175 corresponding to the cationic fragments $[\mathbf{L1}I]^+$ ($[C_9H_{12}IN_4Se_2]^+$), $[\mathbf{L1}]^+$ ($[C_9H_{12}N_4Se_2]^+$) and $[C_5H_7N_2Se]^+$, respectively, with a very good fitting of the isotopic pattern [see Figure S1 in the Supplementary Information (SI)]. A yellow powder corresponding to the formulation $[\mathbf{L1}Se](I)_2$ was recovered (45.3% yield) from the filtered yellowish solid formed at the end of the

reaction of **L1** and I_2 in the presence of Se powder. The ESI-MS spectrum in positive ion mode showed a peak at *m/z*: 541 attributed to the species $[\mathbf{L1}SeI]^+$ ($[C_9H_{12}IN_4Se_3]^+$) and a peak at *m/z*: 644 due to the adduct $[\mathbf{L1}SeI+Se+Na]^+$ ($[C_9H_{12}IN_4Se_3 +Se +Na]^+$) were observed; the fitting of the respective isotopic pattern confirmed their nature (see Figure S2 in the SI). Yellow tablets were obtained from slow evaporation of a MeCN solution of this yellow powder, for which an X-ray diffraction analysis confirmed the same nature as the crystals isolated from the reaction of **L1** and I_2 in the absence of Se powder (compound **III** in Scheme 4). No evidence of $[\mathbf{L1'}](I)_2$ (compound **I** in Scheme 4) formation was observed in the reaction of **L1** with I_2 in MeCN in the presence of Se powder.

The X-ray crystal structure analysis established an ionic character for compound **I** (Scheme 4, see Table S1 in the SI for crystallographic information), the dication $[\mathbf{L1'}]^{2+}$ being balanced by two I^- anions. The formation of $[\mathbf{L1'}]^{2+}$ is presumably the result of a deselenation process **L1** undergoes in the reaction mixture followed by an intramolecular ring-closure with the formation of a six-membered ring, favoured by the polarity of the solvent and the oxidizing nature of I_2 under the experimental conditions used. The $[\mathbf{L1'}]^{2+}$ dication lies on a crystallographic mirror plane; the asymmetric unit consists of two half-dications bridged by an $\mathbf{I^-}$ anion (I1), with two additional $\mathbf{I^-}$ anions (I2 and I3) located on special positions (a two-fold screw axis and a mirror plane, respectively) with occupancy 0.5 (Figure 1).

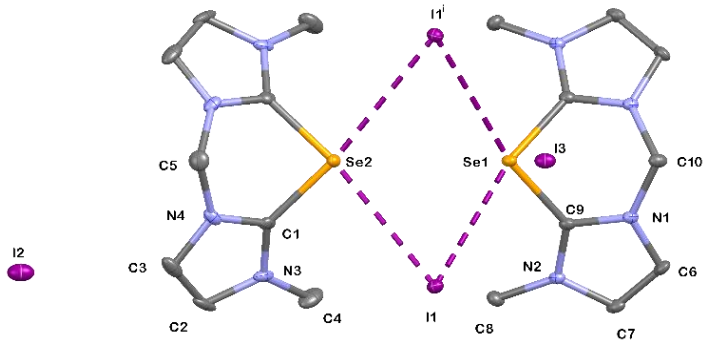

Figure 1. View of the molecular structure of compound **I** ($[\mathbf{L1'}](I)_2$) with the atom labelling scheme adopted. Displacement ellipsoids are drawn at 50% probability level and hydrogen atoms are omitted for clarity. Symmetry operation: ^{i} = +x, +y, 1−z. Selected bond lengths (Å) and angles (º) are reported in Table S2 (SI).

The [**L1'**]$^{2+}$ dication features a folded conformation resembling an open book, with the spine along the line connecting the methylene carbon (bridging the two five-membered rings) and the Se atom. This shape involves a boat conformation of the central six-membered ring, with dihedral angles between the two planar imidazoline rings of 61.95(12)^{o} and 65.23(13)^{o}. Two [**L1'**]$^{2+}$ units are bridged by two iodide anions with the formation of a tetranuclear [Se_2I_2] cyclic core (Figure 1). The Se–I distances are quite long [Se1–I1 = 3.4771(2), Se2–I1 3.4737(2) Å] and only slightly shorter than the sum of the relevant van der Waals radii [ΣrvdW (Se,I) = 3.88 Å],[32] in agreement with a marked ionic character of compound **I**.

Adjacent [(**L1'**)$_2$(I)$_2$]$^{2+}$ dimeric units are joined by C−H···I contacts of 2.88 Å between two symmetry-related C3−H3 groups and iodide anions (I2) in an $R(16)_4^2$ motif to form ribbons parallel to the [100] direction (Figure 2). The extended crystal packing features [(**L1'**)$_2$(I)$_4$]$_n^{n+}$ ribbons and columns of iodide anions (I3), parallel to but not interacting with each other (Figure S3 in the SI).

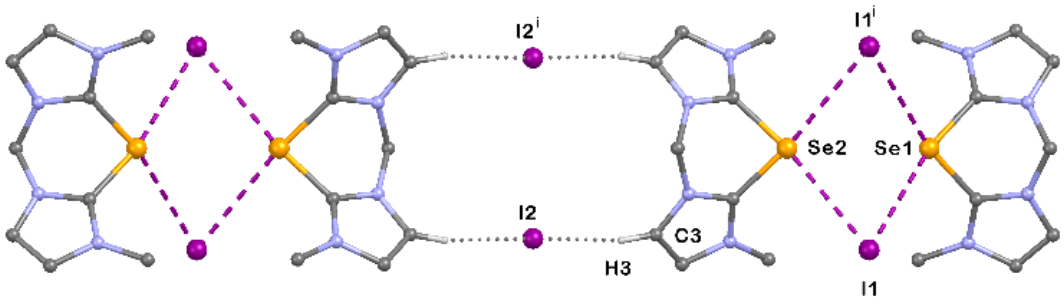

Figure 2. View along the [100] direction of the weak C−H···I contacts found in compound **I** with the labelling scheme adopted. (C3−H3···I2): C3···I2 3.793(3), C3−H3 0.95; H3···I2 2.88 Å, C3−H3−I2 = 160°. Only interacting hydrogen atoms are shown for clarity. Symmetry operation: ^{i} = +x, +y, 1−z.

A deselenation process in the reactions of selenoamides with oxidizing agents is rare, but not unknown (see Scheme S1 in the SI for some examples concerning cyclic selenoamides). In particular, the reaction of **L1** and **L2** with tetracyanoquinodimethane (TCNQ) afforded the semiconducting mixed valence compounds [**L1'**](TCNQ)$_3$ and [**L2**]$_3$[(TCNQ)$_3$]$_2$.[33, 34] In [**L1'**](TCNQ)$_3$ the same dication observed in **I** was found following deselenation of **L1** (Scheme S1), while in [**L2**]$_3$[(TCNQ)$_3$]$_2$ two [**L2**]$^{2+}$ cyclic dications featuring an intramolecular Se–Se bond (see below)

interact with the Se atoms of a bridging neutral donor molecule **L2** to afford Se–Se–Se three-body systems (Scheme S2).

Single crystal X-ray diffraction analysis established an ionic character also for compound **II**, characterized by the presence in the crystal lattice of polymeric $[\mathbf{L1}I]_n^{n+}$ poly-cations balanced by I^- anions (see Table S1 in the SI for crystallographic information). The cationic repeating unit $[\mathbf{L1}I]^+$ lies on a crystallographic mirror plane with the asymmetric unit consisting of half an **L1** ligand interacting with an I^+ cation (I1) balanced by an I^- anion (I2), both located on special positions (a glide plane and a two-fold screw axis, respectively) with occupancy of 0.5 (Figure 3).

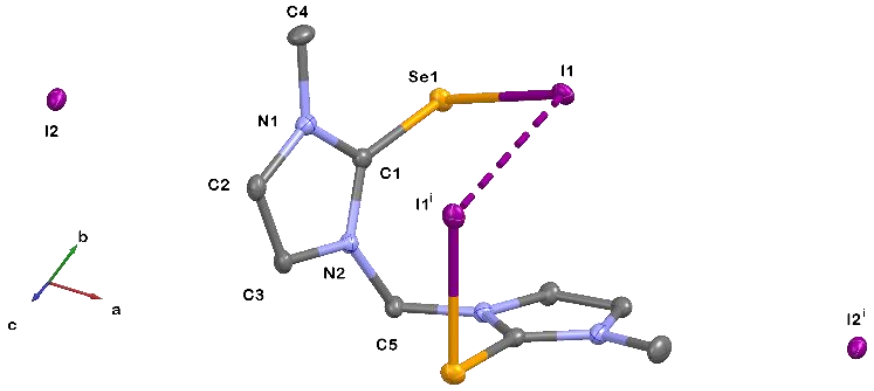

Figure 3. View of the molecular structure of compound **II** ($[\mathbf{L1}I]_n(I)_n$) with the atom labelling scheme adopted. Displacement ellipsoids are drawn at 50% probability level and hydrogen atoms are omitted for clarity. Symmetry operation: ^{i} = 1−*x*, +*y*, 3/2−*z*. Selected bond lengths (Å) and angles (°) are reported in Table S3 (SI).

Each I^+ centre bridges two Se atoms from different **L1** ligand moieties, thus forming a polymeric $[\mathbf{L1}I]_n^{n+}$ 1D-chain running along the [101] direction (Figure 4). Therefore, each **L1** ligand unit is bound to two I^+ centres in a κ^1-fashion (the two Se-donor atoms interact with two different I^+ cations) and assuming a conformation that makes the two C=Se groups *syn-anti* oriented with respect to the plane containing the N2−C5−N2^i framework (^{i} = 1−*x*, +*y*, 3/2−*z*, Figures 3 and 4).

Alternatively, the $[\mathbf{L1}I]_n^{n+}$ poly-cations in **II** can be seen as poly-iodonium complexes of iodine(I) atoms (I1) coordinated by two chalcogen atoms from two 4-imidazoline-2-selone

moieties bridged by a methylene group. Accordingly, the Se–I bond distance of 2.7763(3) Å is close to that observed in other iodonium complexes of selone donors.[20] Compound **II** represents the first example of an iodonium complex of imidazoline-2-selone derivatives, which most commonly afford "T-shaped" I_2-adducts and diselenide cations when reacted with di-iodine (see above).

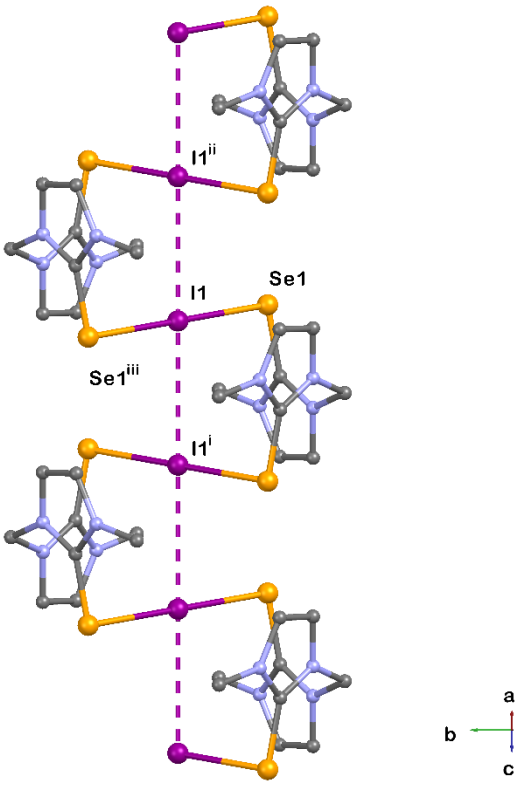

Figure 4. Partial view of a polymeric $[\mathbf{L1}I]_n^{n+}$ 1D-chain along the [101] direction in compound **II**. Symmetry operations: ^{i} = 1−*x*, +*y*, 3/2−*z*; ^{ii} = +*x*, 1−*y*, −½+*z*; ^{iii} = 1−*x*, 1−*y*, 1−*z*.

Very few spectroscopic data are available for iodonium complexes featuring a Se–I–Se three-body system, and generally the FT-Raman spectra are dominated by the peaks from the polyiodide counter-anions.[20, 35] On the ground of a Se/Br mass similarity, the Raman peaks for the stretching vibrations of the Se–I–Se three-body system are expected to occur at frequencies close to those observed for Se–I–Br fragments in CT IBr-adducts with Se-donors or Br_3^- and IBr_2^- trihalides.[21a, 35] Therefore, a symmetric or slightly asymmetric Se–I–Se group should give rise to a peak in the range 140-160 cm^{-1}, typical for Br_3^- and IBr_2^- trihalides. The FT-Raman spectrum of compound **II** exhibits a peak at 133.5 cm^{-1} (with a

shoulder at 145 cm^{-1}), which can be tentatively assigned to the symmetric stretching vibration mode of the Se–I–Se three-body system, and a much weaker peak at 183.5 cm^{-1} (Figure S4 in the SI). Similar FT-Raman spectra were recorded for the symmetric iodonium complexes [(^{t}Bu$_2$^{i}PrPSe)$_2$I]I_3 and [(^{i}Pr$_3$PSe)$_2$I]I_3 of trialkylphosphane selenides,[35] which, however, are dominated by the bands from the I_3^- counter-anions. Furthermore, a ^{77}Se{^{1}H} spectrum of **II** recorded in DMSO-d_6 (see the Experimental Section) shows only one signal at 162.08 ppm with respect to H_2SeO_3 (downfield shifted with respect to signal at 37.59 ppm for **L1** in the same solvent),[15b] which is within the range 107-249 ppm reported for iodonium complexes of 1-(2-bromobenzyl)-3-alkyl-1H-benzo[d]imidazole-2(3H)-selone.[21c]

The X-ray diffraction analysis of compound **III** (Scheme 4) affirms its ionic nature (see Table S1 in the SI for crystallographic information). The cyclic dication [**L1**(μ-Se)]$^{2+}$ (Figure 5) is counter-balanced by two I^- anions.

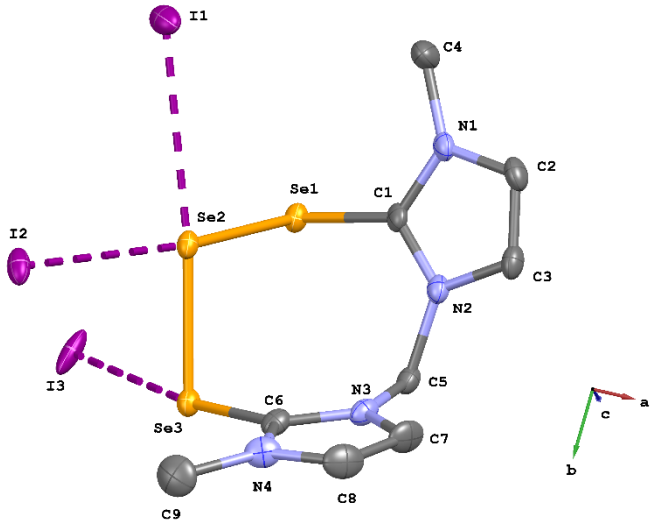

Figure 5. View of the asymmetric unit in compound **III** ([**L1**(μ-Se)](I)$_2$·½H_2O) with the atom labelling scheme adopted. Only one component of the disordered I3 anion lying on the inversion centre is shown. Displacement ellipsoids are drawn at 50% probability level; hydrogen atoms and co-crystallized water molecules are omitted for clarity. Selected bond lengths (Å) and angles (°) are reported in Table S4 (SI).

Beside [**L1**(μ-Se)]$^{2+}$, the asymmetric unit of **III** features an I^- anion (I1), and two additional I^- anions (I2 and I3) located on special positions (centres of inversion) with fractional occupancy 0.5 (Figure 5). However, I3 is disordered over its inversion centre, and the structure also contains half H_2O

molecules disordered over two sites (see the Experimental Section and Figure S5 (SI). In [**L1**(μ-Se)]$^{2+}$, **L1** formally chelates a selenium(II) centre (Se2 in Figure 5) in a κ^2-fashion (the two Se-donor atoms both coordinating Se2), thus assuming a conformation that brings the two C=Se groups into a *syn* orientation with respect to the plane containing the N2–C5–N3 framework (Figure 5).

The cyclic [**L1**(μ-Se)]$^{2+}$ dication interacts at the chelate selenium(II) centre (Se2) with the I^- anions I1 and I2 at distances of 3.4231(4) (Se2−I1) and 3.3717(3) Å (Se2−I2), respectively, which are only slightly shorter than the sum of the relevant van der Waals radii [ΣrvdW (Se,I) = 3.88 Å];[32] a longer interaction of 3.5359(3) Å, almost at the limit of the sum of the van der Waals radii, is observed between the selenium atom S3 belonging to **L1** and the I3 iodide (Figure 5), in agreement with a strong ionic character of compound **III**.

A distorted square planar *cis*-Se_2SeI_2 group is formed as part of a puckered eight-membered heterocycle featuring similar Se−Se bonds [2.3936(5) and 2.3921(5) Å for Se1−Se2 and Se2−Se3, respectively) and Se−Se−I angles (88.132(13) and 88.057(12)^o for Se1−Se2−I1 and Se3−Se2−I2, respectively; 173.040(16) and 174.580(15)^o for Se1−Se2−I2 and Se3−Se2−I1, respectively]. The planar *cis*-Se_2SeI_2 group is almost perpendicular to the planes containing the imidazoline moieties [C1−Se1−Se2 = 97.80(9)^o; C6−Se3−Se2 = 95.58(10)^o] and to the direction defined by the S3−I3 interaction [I3−Se3−Se2 = 81.955(12)^o, C6−Se3−I3 = 166.11(10)^o] (Figure 5). To the best of our knowledge, compound **III** represents the first example of a dicationic [RSeSeSeR] triselane consisting of one **L1** unit chelated to a Se^{2+} cation. Only neutral [RSeSeSeR] systems are documented in the literature, with the exception of the compound [$N(PPh_2Se)_2$(μ-Se)](I)[36] whose structure consists of two cyclic six-membered [$N(PPh_2Se)_2$(μ-Se)]$^+$ cations in a chair conformation and two bridging I^- anions in a disposition similar to that observed in compound **I**. Interestingly, the Se–Se bond distances in [**L1**(μ-Se)]$^{2+}$ [2.3936(5) and 2.3921(5) Å, Table S4] are shorter than those observed in [$N(PPh_2Se)_2$(μ-Se)]$^+$ [2.441(1), 2.427(1) Å] despite the fact that in the latter the chelating ligand is monoanionic and not neutral.[36] The C–Se bond lengths (1.891(3) and 1.900(3) Å for C1–Se1 and

C6–Se3, respectively, Table S4) are very close to that observed in **II** (1.870(2) Å, Table S3) and slightly longer than those reported for free **L1** [1.842(4) and 1.853(3) Å].[37]

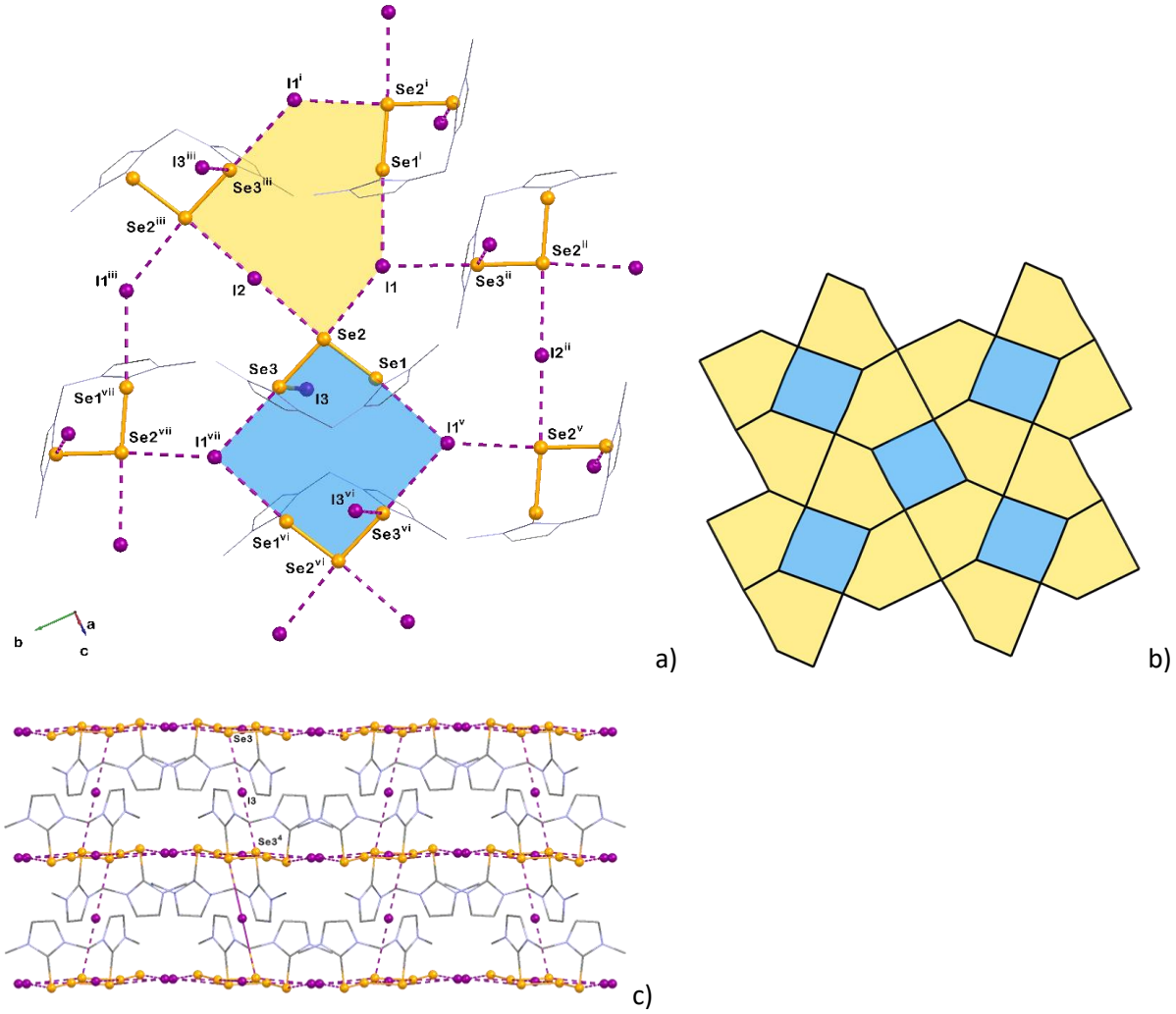

Figure 6. a) Partial view of the 2D-network formed from the interaction of [**L1**(μ-Se)]$^{2+}$ dications and I1 and I2 iodide anions; b) pictorial representation of the 2D-network as a tiled pattern of irregular squares (blue) and pentagons (yellow); c) partial view of the packing diagram along the [101] direction showing I3 bridges between adjacent layers. Symmetry codes: i = −½+x, ½−y, −½+z; ii = ½−x, −½+y, 3/2−z; iii = −x, 1−y,1−z; iv = −x, 1−y, 2−z; v = ½+x, ½−y, ½+z; vi = 1−x; 1−y; 1−z; vii = ½−x; ½+y; ½2−z.

Each I$^-$ anion (I1, I2 and I3) in **III**, interacts with symmetry-related [**L1**(μ-Se)]$^{2+}$ dications, with I−Se distances ranging between 3.3717(3) and 3.5629(4) Å (Figure 6 and Figure S6 in the SI). Layers of interacting –Se_3– moieties (from [**L1**(μ-Se)]$^{2+}$ dications) and iodide anions, form a 2D-network lyingin the (101) plane and perpendicular to the [010] direction. Two distinct geometrical motifs can be identified in the 2D-network, both featuring Se_6I_2 eight-membered rings, which derive from I1 and

Se2 acting as three- and four-junction nodes, respectively, and I2, Se1 and Se3 acting as two-junction nodes. Each overall Se_6I_2 pseudo-square motif (indicated as light-blue tile(s) in Figures 6a and 6b) is fused with four Se_5I_3 irregular pentagon motifs (indicated as yellow tile(s) in Figures 6a and 6b) to give regular and planar tiled arrangements perpendicular to the [010] direction (Figure 6b). I3 iodide anions connect adjacent parallel layers featuring this tiled pattern of irregular square and pentagon shapes by interacting with two symmetry-related Se3 atoms from triselane moieties (Figure 6c) located on adjacent layers. The space between the layers (the inter-layer distance is approximatively 15 Å) is occupied by the organic portion of the [**L1**(μ-Se)]$^{2+}$ dications.

The FT-Raman spectrum of **III** (Figure S7 in the SI) in the low frequency region is characterized by a broad band at 230 cm^{-1} with a shoulder at 215 cm^{-1}. These bands can be attributed to the ν(Se−Se) stretching vibrations within the triselane moiety of **III** and correlate well with the bands observed at 195 and 255 cm^{-1} for the mono-cation [N(P^{i}Pr$_2$Se)$_2$]$^+$ as I$^-$ and SbF_6^- salts, respectively,[36] which exhibit Se−Se bond lengths of 2.484(1) and 2.348(1) Å, respectively. A Raman band at 270 cm^{-1} has been recorded for the neutral compound $Se_3(CN)_2$, in which the Se−Se bond length is 2.3390(7) Å.[38] Interestingly, the reaction of **L1** with I_2 in 1:2 molar ratio in MeCN afforded in good yield, upon slow evaporation of the solvent dark red block-shaped crystals having an analytical formulation different from that of **I**–**III**, and a structured FT-Raman spectrum in the low frequency region (see below). The ESI-MS spectrum in positive ion mode exhibited a peak at m/z: 463 corresponding to the cationic fragment [**L1**I]$^+$ ([$C_9H_{12}IN_4Se_2$]$^+$) as confirmed by the fitting of the isotopic pattern (see Figures S8-S9 in the SI). An X-ray diffraction analysis allowed establishing the formulation [**L1**I](I_3)·2I2 (**IV**) for the isolated compound (Figure 7).

Compound **IV** is at the same time an "extended spoke" CT adduct of the type RSe−I_2−I_2 and a triiodide salt of an [RSe–I]$^+$ cation (R = organic framework). In **IV**, the ligand **L1** assumes a conformation recalling that observed in **II**, with two C=Se groups assuming a *syn-anti* orientation with respect to the plane containing the N2−C5−N3 moiety.

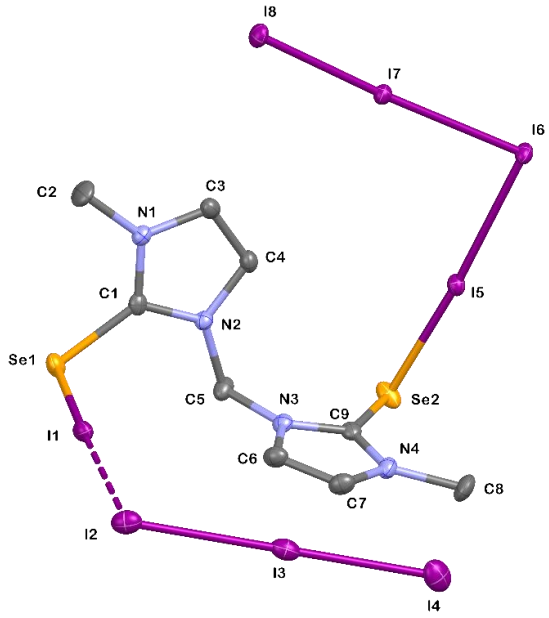

Figure 7. View of the molecular structure of compound **IV**, [**L1**I](I$_3$)·2I$_2$, with the atom labelling scheme adopted. Displacement ellipsoids are drawn at 50% probability level and hydrogen atoms are omitted for clarity. Selected bond lengths (Å) and angles (°) are reported in Table S5 (SI).

The C9=Se2 chalcogenone group is involved in the formation of an "extended spoke" CT adduct with two I$_2$ molecules (Figure 7). The di-iodine molecule directly bound to the Se atom [Se2–I5 = 2.6591(4), I5–I6 = 3.0375(3) Å; Se2–I5–I6 176.149(10)°] is almost perpendicular to the C–Se bond [C9–Se2–I5 = 93.39(8)°] and interacts *via* the terminal iodine atom I6 with a second molecule of I$_2$ [I6–I7 = 3.0497(3), I7–I8 = 2.8064(3); I6–I7–I8 = 175.839(8)°]. The I5–I6–I7 angle is very close to 90° [95.876(7)°] according to the CT molecular orbital scheme which involves donation from one of the filled π* orbitals of the I$_2$ molecule coordinated to the chalcogen atom to the σ* orbital of the second I$_2$ molecule. The pattern of Se–I and I–I distances clearly shows a strong donation from the chalcogenone (C9=Se2) moiety with a significant reduction of the bond order in the I$_2$ molecule directly bonded to the Se atom. The terminal I (I6) atom of the latter interacts weakly with the second I$_2$ molecule (I7–I8), which is thus slightly elongated. The second chalcogenone moiety of **L1** in **IV** (C1=Se1, Figure 7) is also involved in a CT interaction of the type RSe→I$_2$→I$_2$ with two di-iodine molecules, typical of "extended spoke" CT adducts. However, the interaction between the Se atom and the first I$_2$ molecule is so strong that the I–I bond (I1–I2 in Figure 7) lengthens

to 3.2753(3) Å and the Se1−I1 shortens to 2.6074(4) Å; as a consequence the terminal iodine atom (I2 in Figure 7) interacts with the second I_2 molecule to form an asymmetric I_3^- triiodide [I2−I3 = 2.9972(3), I3−I4 = 2.8694(3) Å; I2−I3−I4 = 178.632(9), I1−I2−I3 = 102.260(8)°]. The whole system can therefore be better described with the ionic formulation $[RSe{-}I]^+\cdots I_3^-$. A similar situation was found in the 1:1 adduct between *N*-methylbenzothiazole-2(*3H*)-selone (btseMe) and IBr,[21a] which can be described as an ion pair $[btseMe{-}I]^+\cdots IBr_2^-$, based on the Se−I and I−Br distances observed in the structure.

This ionic description of the C1−Se1−I1···I2−I3−I4 fragment in **IV**, as compared to the C9−Se2−I5−I6···I7−I8 moiety, is supported by the larger value observed for the C1−Se1−I1 angle [98.33(8)°] with respect to the C9−Se2−I5 angle [93.39(8)°], which is considered a diagnostic structural feature for the formation of a $[RE{-}X]^+$ cation upon interaction of a chalcogen-containing donor and a di-halogen molecule. The >C−Se−I angle for the Husebye's cation $[RE{-}I]^+$, RE = N,N'-dimethyl-4-imidazoline-2-selone, was calculated to be 98.3° (see below).[27]

Units of **IV** interact *via* Se···I contacts to give stair-like ribbons parallel to [001], whose steps are Se_2I_8 ten-membered rings in a chair conformation (Figure 8).

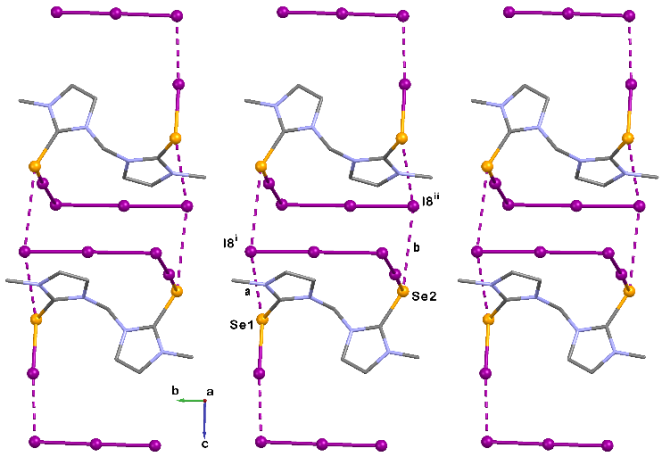

Figure 8. Partial view of **IV** along the [100] direction showing stair-like ribbons of [**L1**I](I_3)·2I_2 units interacting *via* Se···I contacts: Se1···I8^{i} = 3.5799(4), Se2···I8^{ii} = 3.8120(4). Symmetry codes: ^{i} = −1+x, +y,+z; ^{ii} = 1−x,1−y,−z.

The reactivity of **L2** with I_2 in MeCN was also investigated. The reaction of **L2** and I_2 in 1:1 molar ratio afforded a crystalline yellow solid corresponding to the formulation **L2**I_2, it was recovered from the reaction mixture (62.4% yield) by filtration after 24 h stirring at room temperature. This solid was crystallized from MeCN to afford single crystals of compound [**L2**]$(I)_2$·MeCN (**V**) as established by X-ray diffraction studies (see below and Scheme 5).

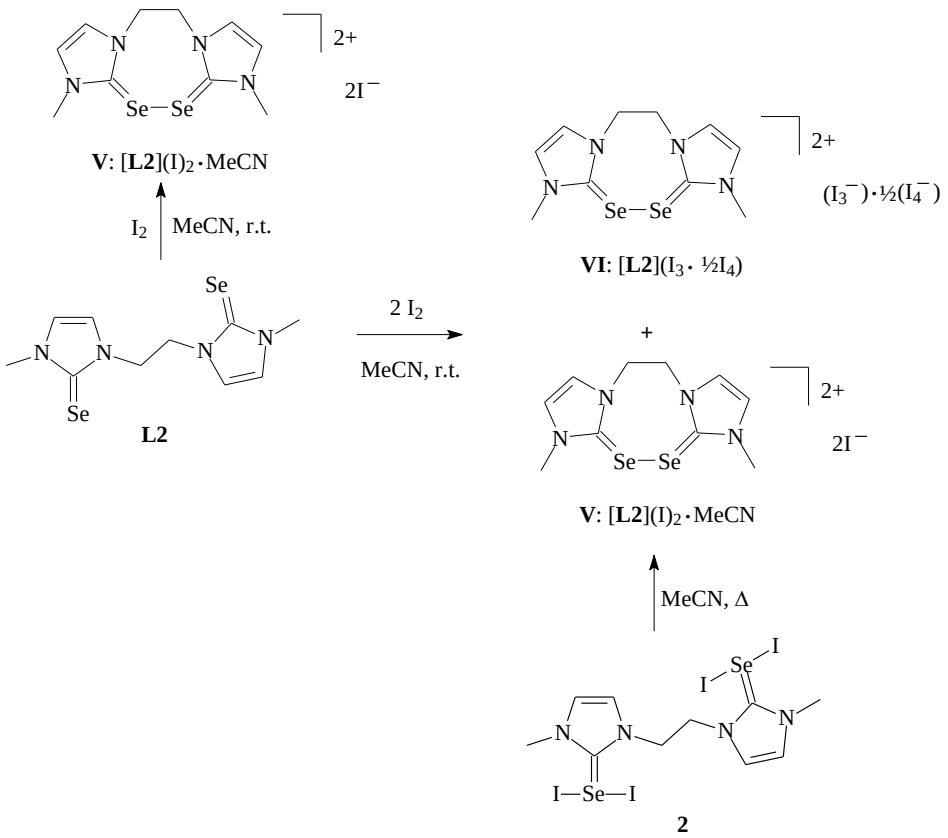

Scheme 5. Compounds isolated from the reaction of **L2** with I_2 in MeCN as established by X-ray diffraction analysis.

The reaction between **L2** and I_2 in 1:2 molar ratio under the same experimental conditions afforded a dark red solution from which crystals of compound [**L2**](I_3·½I_4) (**VI**, Scheme 5) were formed by partial evaporation of the solvent (27.3% yield). A further evaporation of the solution from the first crystallization afforded a mixture of single crystals of **V** and **VI** as established by X-ray diffraction analysis and ESI-MS spectrum in positive ion mode (both compounds exhibit the main peak at m/z: 477 corresponding to the cationic fragment [**L2**I]$^+$ ($[C_{10}H_{14}IN_4Se_2]^+$), see Figures S11-S14 in the SI) and X-ray diffraction analysis. Both **V** and

VI exhibit one signal in the $^{77}Se\{^{1}H\}$ spectrum recorded in DMSO-d_6 at 298.93 and 341.36 ppm with respect to H_2SeO_3, respectively (downfield shifted with respect to signal at 27.27 ppm for **L2** in the same solvent),[15b] and quite close to the value of 343,31 ppm of a broad signal recorded for **IV**, which appears to point out a similar nature of the species formed in MeCN solution from **L1**(**L2**)/I_2 mixtures. A $^{77}Se\{^{1}H\}$ signal at 329.25 ppm with respect Me_2Se in CD_3CN was recorded for the diselenide dication of N,N′-dimethyl-4-imidazoline-2-selone.[8a]

A similar mixture of **V** and **VI** was also obtained both on cooling down a hot MeCN solution of **2** (Scheme 5), see Experimental Section, and treating **2** with 2 equivs. of elemental Te in Et_2O at room temperature for 2 weeks, followed by crystallization from hot MeCN of the solid residue recovered by filtration.[14a]

While for compound **VI** the spectroscopic characterization and the X-ray crystal structure were already reported in the literature,[14a] the nature of compound **V** had been inferred only from microanalytical and FT-Raman spectroscopic data.[14a] Therefore, we performed a single crystal X-ray crystal diffraction analysis of **V** (see Table S1 in the SI for crystallographic information) that as expected, features a discrete $[\mathbf{L2}]^{2+}$ dication generated by symmetry through a glide plane, in which the Se−Se [2.3961(6) Å, see Table S6 in the SI] intramolecular bond leads to an eight-membered ring with a chair conformations. Two I^- counter-anions located on special positions with occupancy 0.5, and a disordered co-crystallized half MeCN molecule complete the asymmetric unit (see Figure S15 and Table S6 in the SI). Analogously to compound **I**, $[\mathbf{L2}]^{2+}$ units in **VI** are bridged by two iodide anions [Se1−I1 = 3.4856(4), $Se1^{i}$–I2 = 3.5081(4) Å; I1−Se1−$Se1^{i}$ = 163.766(9), $I2^{iii}$–Se1−$Se1^{i}$ = 94.194(11), I1−Se1−$I2^{iii}$ = 99.463(10)°, Se1−I1−$Se1^{iv}$ = 74.896(12)°, Se1−$I2^{iii}$–$Se1^{iv}$ = 74.340(13)°] with the formation of a tetranuclear $[Se_2I_2]$ cyclic core (Figure 9).

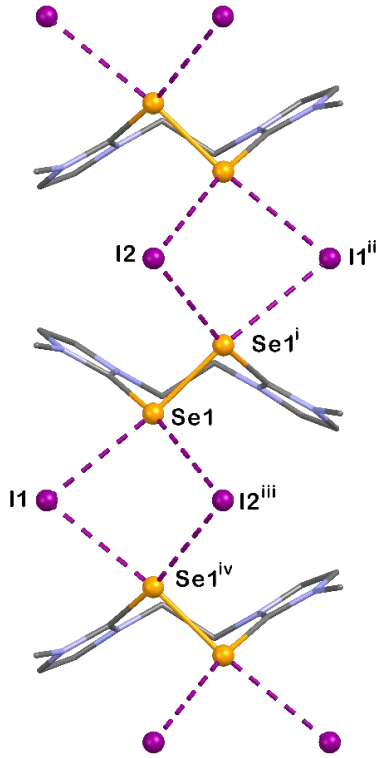

Figure 9. Partial view along the [100] direction of a stair-like ribbon of alternating [**L2**]$^{2+}$ dications and I^- anions in compound **VI**. Symmetry codes: ^{i} = +*x*, ½−*y*, 1−*z*; ^{ii} = +*x*, ½−*y*, −½+*z*; ^{iii} = +*x*, ½−*y*, ½+z; ^{iv} = +x, +y, 3/2-z. Selected bond lengths (Å) and angles (º) are reported in Table S6 (SI).

As both Se atoms of each dication are involved in this I^- bridging interactions, stair-like ribbons of alternating [Se_2I_2] cycles and [**L2**]$^{2+}$ dications are formed along the [001] direction. As in the case of **L1**, we also performed the reaction of **L2** with I_2 in 1:1 molar ratio d in the presence of one equiv. of Se powder under the same experimental conditions. A yellow solid was recovered (see Experimental Section) corresponding to the formulation [**L2**Se](I)$_2$, which features in the ESI(+)-MS spectrum a weak molecular peak at *m/z*: 681 corresponding to the cationic fragment [**L2**SeI_2-H]$^+$ ([$C_{10}H_{14}IN_4Se_2$]$^+$), (see Figure S16 in the SI). The FT-Raman spectrum show the main peak at 229 cm^{-1} in good agreement with the band observed at 230 cm^{-1} for compound **III** ([**L1**(μ-Se)](I)$_2$·½H_2O) (see above, Figure S17). Unfortunately, despite numerous attempts, we were not able to grow single crystals of this compound.

DFT theoretical calculations

In order to better understand the nature of the products obtained by reacting **L1** and **L2** with molecular di-iodine and the effects played by the solvent, theoretical calculations were carried out at the Density Functional Theory level.[39] Theoretical calculations were carried out using: (a) a previously adopted set-up [mPW1PW[40]/ LanL08(d)[41] for iodine and selenium; def2-SVP[42] for lighter atomic species] that provided very reliable results for a variety of different molecular systems, including halogen-rich products;[28, 43] (b) the highly parametrized M06-2X functional[44] coupled with the same basis sets; (c) the M06-2X functional with the aug-cc-pVTZ[45] for all atomic species except iodine, for which the aug-cc-pVTZ-PP[45] basis set was adopted including further polarization functions. This last set-up is meant to be particularly well-suited for investigating weak interactions, such as chalcogen (ChB) and halogen bond (XB) σ-hole interactions, and it has been reported to provide computational results comparable to those achieved with an *ab initio* post-Hartree-Fock Möller-Plesset (MP) perturbative approach.[46, 47]

A comparison of the calculated structural features of the CT "spoke" adduct **L1**·2I_2 with the available structural data[14b] (Table S7 in the SI) shows that DFT calculations underestimate the CT interaction between the selone donor and I_2, with longer optimized Se···I (by up to 9.5%) and shorter I–I (up to 6%) optimized bond distances as compared to the structural data. The metric parameters of "T-shaped" adducts are better reproduced. In accordance with structural evidence (Table S7 in the SI), the two Se–I distances are different to each other, the C–Se–I angle increasing with the shortening of the corresponding Se–I distance. On the average, the setup (a) provides more reliable bond distances and angles, confirming the results previously reported.[43] For this reason, although all calculations discussed below have been carried out with all the three set-up, only those obtained with the mPW1PW functional will be discussed here.

In order to examine the nature of compounds **I**–**VI** (see above), a few simpler model compounds were optimized in the gas phase and in MeCESIN and CH_2Cl_2 solution (Table S8 in the SI), the solvents being implicitly accounted for by means of the polarizable continuum model in its integral equation

formalism (IEF-PCM),[48] describing the cavity of the complexes within the reaction field (SCRF) through a set of overlapping spheres.

N,*N*'-Disubstituted imidazoline-2-chalcogenone derivatives feature two lone pairs (LPs) of electrons localized on the chalcogen atom and available for donation towards Lewis acids. The molecular orbitals (MOs) in the range HOMO-3–HOMO exhibit the four possible combinations of the two LPs (see Fig. S18 in the SI for the Kohn-Sham (KS) HOMO of **L1**). When the acceptor is a di-halogen or inter-halogen both CT "spoke" adducts and "T-shaped" hypercoordinate complexes of the chalcogen atom can be formed. The stability of the two types of products depends on the structure of the chalcogen donor molecule and the di-halogen species. In the case of bis-4-imidazoline-2-selone derivatives, both types of adducts where indeed isolated and characterised structurally (see above). Accordingly, the free energy associated with the adducts formation, as calculated from thermochemical data is indeed very close (–9.72 and –12.70 kcal mol^{-1} for the "spoke" and "T-shaped" **L1**·$2I_2$ adducts, respectively, in the gas phase at 298 K; Fig. S19 and Table S9 in the SI). It is worth recalling that the formation of the CT "spoke" adduct is probably the first step in the interaction for any type of isolable product, and the interconversion between "spoke" and "T-shaped" adducts does not require the detachment of a halide species.[49] This notwithstanding, when the interaction of the donor to di-iodine is strong enough, the CT process could bring about a strong polarization of the I–I bond of the initially coordinated di-iodine molecule leading to $[RE–I]^{\delta+}\cdots I^{\delta-}$ species in solution, as recently demonstrated in the case of the products isolated from the reaction of 1,3-dimethyl-4-imidazoline-2-thione with di-iodine.[50] As mentioned above, the cation $[RE–I]^{+}$, which might formally originate from either the initially formed CT or "T-shaped" adducts by heterolytic cleavage of the X–X or E–X bond, has proved to be a useful model to investigate/predict the final outcome of the reaction of a chalcogen donor RE with IX di-halogens/inter-halogens (X = Cl, Br, I), supporting the reactivity towards I_2 shown in Scheme 2. In fact, the KS-LUMO of this cation is an antibonding σ^{*}-MO localized on the chalcogen–halogen bond, available to receive electron density at both chalcogen and halogen atom sites (see Fig. S20 in the SI for **L** = **L1**). The

charge distribution calculated at NBO[51] level can indicate which of the two sites in the $[RE–I]^+$ cation would preferentially undergo a nucleophilic attack (for example by $I^–$) thus defining the final product:[25, 28] when the positive charge is mainly located on the chalcogen atom of the $[RE–I]^+$ cation, the formation of the "T-shaped" adduct would be favoured, while the CT adduct would preferably form when the positive charge is located on the terminal halogen atom.[25] In the case of **L1** (and in general of 4-imidazoline-2-chalcogenone systems)[25, 28] the dication $[\mathbf{L1}(I)_2]^{2+}$ features a more positive natural charge localized on the Se atoms than on the I atoms (Q_{Se} = +0.298; Q_I = 0.095 |e|, see Table S8 in the SI), indicating a preferred formation of the "T-shaped" adduct in the reaction with di-halogens and inter-halogens, in agreement with the structure of compound **2** isolated from the reaction of **L1** and I_2 in CH_2Cl_2 (Scheme 3). However, the charge difference between Se and I is modest ($\Delta Q_{Se–I}$ = 0.203 |e|) and the two types of adducts show very similar energies in the gas phase, differing by less than 6 kcal $mol^{–1}$, so that solvation or packing effects could become relevant in stabilizing one of the two adducts. In fact, **L2** affords the CT "spoke" adduct under the same experimental conditions (Scheme 3). On the other hand, the chalcogen atom in the cation $[RE–I]^+$, can be considered as a chalcogen bond (ChB) donor,[52] while the terminal halogen atom as a halogen bond (XB) donor. Therefore, the nature of the final product of the reaction of chalcogenone donors and I_2 can be also seen as the result of a competition between ChB and XB formation with the nucleophile (*e.g.* $I^–$). Molecular Electrostatic Potential (MEP) maps represent a useful tool to evaluate such competition.[46, 50, 52] In Figure 10, the MEP map of the $[\mathbf{L1}(I)_2]^{2+}$ dication is represented, showing the most negative potential to be located on the halogen atom, thus further confirming a preferential nucleophilic attack at the chalcogen site.

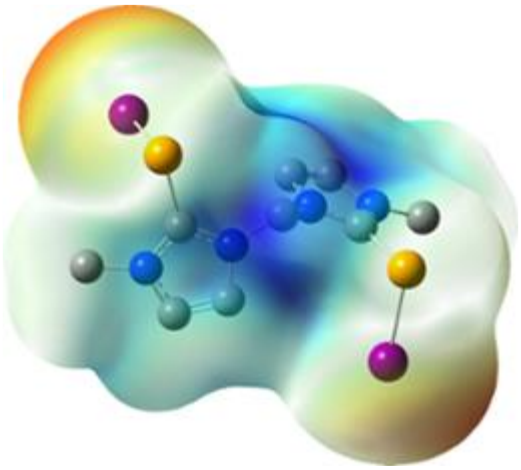

Figure 10. MEP map calculated for [**L1**$(I)_2]^{2+}$ at DFT level (range +0.150 (red)–0.265(blue) kJ/mol). Hydrogen atoms were omitted for clarity.

The "T-shaped" and the CT "spoke" adducts, **L1**·$2I_2$ (CT/T-sh), and the dication [**L1**$(I)_2]^{2+}$, were also optimized by implicitly considering the effect of solvation in MeCN and CH_2Cl_2 at IEF-PCM SCRF level. An examination of the natural charge distribution on the dication [**L1**$(I)_2]^{2+}$ (Table S8 in the SI) indicates that the polarization of the Se–I bond slightly increases along the series gas phase < DCM < MeCN, the charge separation between selenium and iodine passing from 0.203 to 0.278 |e| in the gas phase and in MeCN, respectively.

This is largely due to an increase in the charge located on the Se atom, which therefore is the most electrophilic site of the [**L1**$(I)_2]^{2+}$ dication both in the gas phase and when solvation is considered. Solvation also increases the polarization of the chemical bonding system in I_2-adducts. In the case of the CT adduct, an increase in the amount of natural charge transferred from the Se donor atoms of **L1** to the di-iodine units (Q_{CT} = 0.331, 0.523, and 0.552 |e| in the gas phase, in CH_2Cl_2, and MeCN, respectively) is calculated, with a consequent elongation of the I–I bonds (2.839, 2.965, and 3.007 Å in the gas phase, in CH_2Cl_2, and MeCN, respectively; Table S8 in the SI). As the CT increases, the I–I molecule becomes progressively more polarized (ΔQ_{I-I} = 0.159, 0.357, and 0.394 |e| in the gas phase, in CH_2Cl_2, and MeCN, respectively; Table S8 in the SI). In the case of **L1**·$2I_2$ (T-shaped), an increase in the polarization of the Se–I bonds is also observed on increasing the polarity of the solvents. Thus, the effect of solvation is to increase the polarization of the bonding system in the considered adducts in dependence of the polarity of the solvent. These considerations clearly support

our initial working hypothesis of a possible higher variety of reaction products when MeCN is used as a solvent than CH_2Cl_2. The difference between the total electronic energies calculated for "T-shaped" and the CT "spoke" adduct **L1**·$2I_2$ decreases on passing from the gas phase to solvated adducts ($\Delta E_{CT-T\text{-}sh}$ = 5.85, 3.97, and 0.53 kcal/mol^{-1} in the gas phase, CH_2Cl_2, and MeCN, respectively), thus further confirming the possible formation of both types of products in solution.

Notably, the shape of KS-HOMO in the CT "spoke" adduct and the negative charge on the terminal iodine atom, which in turn increases in polar solvents with the polarization of the I–I bond in the coordinated di-iodine, allows the adduct **L1**·$2I_2$ (CT) to behave as a Lewis base towards further I_2 acceptor units.

Accordingly, the **L1**·$4I_2$ (CT) "extended spoke" CT adducts was successfully optimized (ΔH_r = –46.21 kcal mol^{-1} at 298 K for the adduct formation starting from **L1**; –16.03 kcal mol^{-1} from **L1**·$2I_2$ (CT) Table S9 in the SI), showing Se→I_2→I_2 interactions patterns with $I_2\cdots I_2$ interactions of 3.165 Å. A comparison of the bond lengths and angles optimized for **L1**·$2I_2$ (CT adduct) and **L1**·$4I_2$ ("extended" CT adduct) shows that the I_2→I_2 interaction leading to the latter adduct strengthens the Se→I_2 donation, resulting in a shortening of the Se–I distance and a lengthening of the I–I distance in the Se-coordinated I_2 molecule on passing from **L1**·$2I_2$ to **L1**·$4I_2$ [d(Se–I) = 2.977 and 2.817 Å for **L1**·$2I_2$ and **L1**·$4I_2$, respectively]. As expected, the terminal di-iodine units are less perturbed and show shorter I–I distance (2.811 Å) than the di-iodine molecules directly bonded to the Se atoms of **L1** (2.944 Å).

The calculations on the previously discussed model compounds allow us to understand better the nature and the structural and spectroscopic features of the compounds isolated from the reactions of **L1**/**L2** with di-iodine in MeCN (see above).

Compound **I**, which is the results of a serendipitous deselenation process of **L1** under oxidizing conditions (see Scheme S1 in the SI), features the interaction of the [**L1'**]$^{2+}$ dication with iodides. The MEP map of the dication [**L1'**]$^{2+}$ clearly shows two σ-holes on the selenium atom, roughly aligned opposite to each C–Se bond (Fig. S21a, SI). Therefore, the interaction

with the I1 and I1' iodides depicted in Figure 1 can be interpreted as a σ-hole noncovalent ChB interaction. Alternatively, in a MO approach, the same interaction between the [**L1'**]$^{2+}$ and I^- anions can be seen as a CT interaction, since the KS-LUMO of the cation is largely located on the Se-atom and oriented approximately along the direction of the Se···I interactions (Figure S21b, SI). With the aim of analysing this interaction in more depth, the ensemble [(**L1'**)$_2$(I)$_2$]$^{2+}$ was also optimised, providing metric parameters in very good agreement with the corresponding structural data (optimised metric parameters, in parentheses corresponding structural data: C1–Se2, 1.960 (1.910 Å); Se2···I1^i, 3.232 (3.477 Å); C1–Se2···I1^i 166.88 (166.17°); labelling scheme as in Figure 1). Notably, a Wiberg bond index (WBI)[53] of 0.188 is calculated for the Se···I interaction and a Second Order Perturbation Theory (SOPT) Analysis of Fock Matrix in NBO Basis[51] shows a CT from the LPs of the iodide to the antibonding C–Se NBOs by 10.87 kcal mol^{-1} (45.90 kJ mol^{-1} ; Figure 11).

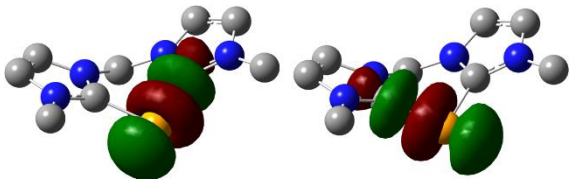

Figure 11. Antibonding C–Se NBOs (isovalue = 0.05 |e|) calculated for [**L1'**]$^{2+}$ at DFT level. Hydrogen atoms were omitted for clarity.

Hence, both the NBO view (reflecting an orbital mixing model) and the σ-hole approach (noncovalent interaction model) can be used to interpret the [**L1'**]$^{2+}$···I^- interactions at the Se atom of the dication, suggesting that both models are able to account for this type of weak interactions.

As regards compound **II**, the [(**L1**)$_2$I]$^+$ model compound was optimised, featuring two symmetry-related **L1** donors, each interacting through a single Se donor with an I^+ cation to form a Se–I–Se linear (179.99°) moiety (optimised Se–I distance 2.830 Å; 2.776 Å observed in compound **II**, Figure 4). In this case also, the formation of the halonium cation can be interpreted as the result of either a σ-hole interaction between I^+ and two Se donor molecules,

or as associated with the formation of a Se–I–Se 3c-4e three-body system. On the other hand, considering the Husebye's cation intermediate, the halonium cation $[(\mathbf{L1})_2I]^+$ in **I** can be considered as derived from $[\mathbf{L1}I]^+$ *via* a nucleophilic attack of a second donor molecule at the halogen site. In the case of compound **II**, the SOPT analysis reveals a CT of 13.85 kcal mol^{-1} with a $WBI_{Se\cdots I}$ = 0.485 very close to the ideal value of 0.5 expected for each bond in a 3c-4e system. A vibrational analysis of $[(\mathbf{L1})_2I]^+$ shows that the Se–I–Se symmetric stretching is combined with various ring vibrations to give the most intense Raman-active peak falling at an unscaled wavenumber of 131.9 cm^{-1}, in agreement with the experimental spectrum (see above, Table S8 and Figure S4, SI).

The $[\mathbf{L1}(\mu\text{-Se})]^{2+}$ dication, isolated in compound **III**, has been singly optimized. In agreement with structural data, the C–Se distance in $[\mathbf{L1}(\mu\text{-Se})]^{2+}$ is elongated with respect to **L1** ($d_{C–Se}$ = 1.892 and 1.841 Å in $[\mathbf{L1}(\mu\text{-Se})]^{2+}$ and **L1**, respectively), and matches almost perfectly the corresponding observed structural values (average C–Se distance 1.895 Å and 1.848 in compound **III**, Figure 5 and Table S4, SI, and **L1**,[37] respectively). This elongation is paralleled by the change in the relevant WBIs ($WBI_{C–Se}$ = 1.056 and 1.323 in $[\mathbf{L1}(\mu\text{-Se})]^{2+}$ and **L1**, respectively). The average Se–Se optimised distance (2.383 Å) is in excellent agreement with the experimental one (2.3936 Å, Table S4 in the SI) in the isolated cation and corresponds to a single bond (average $WBI_{Se–Se}$ = 1.000). The MEP map calculated for $[\mathbf{L1}(\mu\text{-Se})]^{2+}$ (Figure S22, SI) shows two σ-holes on the bridging μ-Se atom (Se2 in Figure 5) disposed opposite to the Se–Se bonds, which categorises the interaction with iodides found in compound **III** as ChBs. Notably, σ-holes are also featured by the Se1 and Se3 atoms, thus accounting for the Se3···I3 interaction (Figure 5 and Figure S5, SI).

In view of the presence of antibonding NBOs localized on the Se1–Se3 and Se2–Se3 bonds, an orbital-mixing interpretation is also possible (Fig. S23 in the SI). When the $[\mathbf{L1}(\mu\text{-Se})](I)_2$ neutral unit is optimised an SeI_2 unit is detached to give an $\mathbf{L1}\cdot SeI_2$ ensemble (Se···Se distance 2.993 Å; $WBI_{Se\cdots Se}$ = 0.253), thus restoring the **L1** ligand. Hence, the structure optimization

of the molecular unit of compound **III** shows that, in contrast to the findings for [**L1'**]$_2$(I)$_2$, the [**L1**(μ-Se)](I)$_2$ ensemble is not stable as such, but only in the complex network of solid-state interactions discussed above. Notably, a vibrational analysis carried out on the cation [**L1**(μ-Se)]$^{2+}$ shows that Se–Se stretching modes, coupled with imidazole ring distortions, are calculated as weak peaks at unscaled frequencies of 222.5 and 285.5 cm^{-1} (Raman activities 5.40 and 8.00 Å/amu, respectively), thus possibly supporting the attribution of the FT-Raman peaks discussed above.

The optimization of the molecular structure of **IV** converged to the **L1**·4I$_2$ (CT) "extended spoke" adduct, displaying two equivalent Se→I$_2$→I$_2$ moieties (see above) both having metric parameters in agreement with only the C9−Se2−I5−I6···I7−I8 fragment in **IV**. The C1−Se1−I1···I2−I3−I4 moiety in **IV** shows for the fragment C1−Se1−I1 bond distances and angles very close to those optimised for [**L1**(I)$_2$]$^{2+}$ dication (Table S8 in the SI). Therefore, DFT calculations confirm the formulation of compound **IV** as [**L1**I](I$_3$)·2I$_2$, proposed on the basis of the direct examination of the structural data. The Raman vibrational analysis of the **L1**·4I$_2$ (CT) "extended spoke" adduct displays for the two different di-iodine units frequencies calculated at about 170 and 160 cm^{-1}, which could be associated in the experimental bands recorded for **IV** at 170 and 145 cm^{-1}, this latter being also contributed by the ν_{as} stretching vibration of the I$_3^-$ counter-anion (Figure S10, SI). The stretching vibration of the Se–I fragment in [**L1**(I)$_2$]$^{2+}$ is calculated at about 240 cm^{-1} (Table S9, SI). When one of the two imidazole-2-selone units interacts with an I$_2$ molecule in the 1:1 model adduct [**L1**I]$^+$·I$_2$, this band is shifted to lower energy by about 10 cm^{-1}. It may be tentatively proposed that a weak contact of the terminal [Se1–I1]$^+$ group with the I$_3^-$ unit, as found in compound **IV** (giving rise to the Se1–I1···I2–I3–I4 moiety), may further weaken the Se–I bond resulting in a shift of its stretching vibration down to the experimental value of 186 cm^{-1} (Figure S10, SI).

The dication [**L2**]$^{2+}$, isolated in compounds **V** and **VI**, was also optimized. As in the previous cases, the optimization converged to metric parameters very close to the structural ones, as

determined by means of the X-ray diffraction characterization. The MEP map (Figure S24, SI) agrees with the NBO view (antibonding NBOs in Figure S25, SI) in indicating the preferential interaction directions of the dication (charge depletion in the MEP) as those opposite to the C–Se and Se–Se bonds, in perfect agreement with the structural features determined for compound **VI** (see Figure 9 and Figure S15 in the SI). Finally, the harmonic vibrational analysis carried out on the cation $[\mathbf{L2}]^{2+}$ shows the Se–Se stretching vibration as the only significant Raman-active peak (unscaled wavenumber ν = 261.23 cm^{-1}; Raman activity 40.29 Å/amu) in the range 50–200 cm^{-1}, thus confirming the attribution previously reported for the experimental FT-Raman band at 229 cm^{-1} (Figure S17, SI).

EXPERIMENTAL

Materials, instrumentation and methods. All syntheses were carried out in air. $\mathbf{L^1}$ and $\mathbf{L^2}$ were prepared according to procedures reported in ref. 14b. Reagents and solvents were used as purchased from Aldrich. Elemental analyses were performed with an EA1108 CHNS-O Fisons instrument (t = 1000 °C). Raman spectroscopy experiments were performed in back-scattered geometry with a non-confocal micro-Raman OEM system. The emission at 785 nm from a fibre-coupled laser diode (BWTEK BRM-785) was focused onto the samples by means of a 10 X objective (laser spot diameter ~ 200 μm). Raman signals were recorded by a fibre-coupled grating spectrometer coupled with a peltier-cooled CCD (BWTEK BTC667N-785S) with spectral resolution better than 5 cm^{-1}. Rayleigh scattering was rejected by means of an edge-filter cutting at nearly 65 cm^{-1}. Depending on the sample under investigation, the laser power was kept below 3 mW to avoid sample melting. No sample decomposition was observed during experiments. The values in parentheses next to the ν(I–I) values represent the intensities of the peaks relative to the strongest, taken equal to 100 (peaks with relative intensities lower than 1 are not reported).

$^{77}Se\{^{1}H\}$ NMR spectra were recorded for solubility reasons in DMSO-d_6 at 25 °C on a Bruker Avance 300 MHz (7.05 T) spectrometer. $^{77}Se\{^{1}H\}$ chemical shifts were referred to H_2SeO_3 (δ 1300 ppm).

Unfortunately, due to insolubility/decomposition reasons for [**L1**(μ-Se)]$(I)_2$ (**III**) and [**L2**Se]$(I)_2$ it was not possible to record a $^{77}Se\{^1H\}$ NMR spectrum even in this solvent.

Mass spectra measurements. Mass spectra were recorded on a triple quadrupole QqQ Varian 310-MS mass spectrometer by using the atmospheric-pressure ESI technique. All the sample solutions were infused into the ESI source with a programmable syringe pump (1.50 mL/h constant flow rate). A dwell time of 14 s was used, and the spectra were accumulated for at least 10 min to increase the signal-to-noise ratio. Mass spectra were recorded in the *m/z* 100 – 1000 range. Scan parameters were chosen to reduce/observe the fragmentation of the metal complexes:[54] needle voltage 3500 V, shield 800 V, source temperature 60 °C, drying gas pressure 20 psi, nebulizing gas pressure 20 psi, detector voltage 1450 V, drying gas temperature 110 °C. Tandem MS experiments were performed using argon as the collision gas (1.8 psi). The collision energy was varied from 5 to 50 V to observe the fragmentation pathways. The isotopic patterns of the measured peaks in the mass spectra were analysed using the mMass 5.5.0 software package.[55] All the mass values are indicated as monoisotopic masses, computed as the sum of the masses of the primary isotope of each atom in the molecule (note that the monoisotopic mass may differ from the nominal molecular mass).

X-ray crystallography. A summary of the crystal data and refinement details for the compounds discussed in this paper are given in Table S1 (SI), only special features are noted here. Single crystal X-ray diffraction data for [**L1'**]$(I)_2$ (**I**), [**L1**I]$_n(I)_n$ (**II**) and [**L1**(μ-Se)]$(I)_2\cdot½H_2O$ (**III**) were collected at 100 K on an Oxford Diffraction Xcalibur, Eos diffractometer, using CrysAlisPro[56] for data collection and processing. Structures of [**L1'**]$(I)_2$ and [**L1**I]$_n(I)_n$ were solved with ShelXS-97.[57] The structure of [**L1**(μ-Se)]$(I)_2\cdot½H_2O$ was solved with ShelXT 2018/2.[58] Data for [**L1**I]$(I_3)\cdot2I_2$ (**IV)** and [**L2**]$(I)_2\cdot$MeCN (**V**) were collected at 100 K and 293 K, respectively, on a Bruker D8 Venture diffractometer equipped with a PHOTON II detector using APEX3[59] for data collection and processing. The structures of [**L1**I]$(I_3)\cdot2I_2$ and [**L2**]$(I)_2\cdot$MeCN were solved with ShelXT 2018/2.[58]

All the crystal structures were refined with ShelXL 2018/3[58] using full matrix least squares minimisation on F^2. Olex2[60] 1.3 and 1.5 were used as the graphical interface.

For [**L1'**]$(I)_2$, a significant peak of residual electron density (*ca.* 3 e/A^3), bonded only to a symmetry-equivalent of itself, could not be interpreted. Possible explanations include disordered solvent (acetonitrile), for which however the void volume is too small, or disordered adventitious water (0.14 molecules), for which there is no other clear evidence. The program SQUEEZE[61] was therefore used to remove mathematically the effects of this peak. The formula and molecular mass (etc.) in Table S1 (SI) do not include any contribution from the supposed "solvent".

For **[L1**(μ-Se)]$(I)_2 \cdot ½H_2O$, one of the iodide anions (I3) was disordered across an inversion centre and was refined over two positions making use of thermal and geometrical restraints. The atomic occupancies for the two components (I3 and I3A) were fixed at 0.22 and 0.28, respectively. Half a water molecule was found co-crystallized in the crystal structure and modelled as a rigid group over two sites with equal atomic occupancies (See Figure S5).

For [**L2**]$(I)_2 \cdot$MeCN, the co-crystallized acetonitrile molecule was disordered across a mirror plane. The solvent molecule was modelled over two sites by means of distance and thermal restraints. The carbon atom of the methyl group (C7) lies on a special position with occupancy 0.5 and is shared by the two parts of the modelled disorder represented by the couples N3–C6 and N3A–C6A, respectively. Atoms N3 and C6 lies on special positions (mirror plane) and their occupancies were fixed at 0.2. The atomic occupancies for N3A and C6A were fixed at 0.3 (See Figure S15 and Table S6, SI).

DFT Calculations. Quantum-mechanical calculations were carried out at Density Functional Theory (DFT)[39] level with the Gaussian[62] commercial suite of computational software. Calculations were carried out at three levels of theory, namely (1) mPW1PW functional[40] and LanL08(d)[41] basis set (BS) for iodine and selenium; def2-SVP[42] for lighter atomic species; (2) M06-2X[44] functional coupled with the same BSs as setup (1); (3) M06-2X[44] functional with the aug-cc-pVTZ[45] for all atomic

species and aug-cc-pVTZ-PP[45] BS for iodine. Basis sets were extracted from the Basis Set Exchange Database.[63] The computational setup was benchmarked by comparing optimized and structural data for **L1**·2I_2 adducts (both CT and "T-shaped" adducts), details of the optimizations are listed in Table S7 in the SI; optimized geometries in Tables S16, S17, S32–S35 in the SI). Based on this benchmark the former setup was eventually chosen. Calculations were extended to **L1**, [**L2**]$^{2+}$, [**L1'**]$^{2+}$, [**L1**(I_2)$_2$]$^{2+}$, **L1**·4I_2, [(**L1**)$_2$I]$^+$, [**L1**I]$^+$·I_2, [**L1**(μ-Se)]$^{2+}$, [**L1**(μ-Se)](I_2)$_2$, [(**L1'**)$_2$(I_2)$_2$]$^{2+}$ (optimized geometries in Tables S12–S23 in the SI), in addition to a selection of iodo species (I^+, I^-, I_2, I_3^-; Table S8–S11 in the SI). For all the investigated compounds the geometries were optimized, starting from structural data when available. To determine the influence of the solvent on the properties of the investigated compounds, calculations for [**L1**(I_2)$_2$]$^{2+}$, **L1**·2I_2 (CT "spoke" and "T-shaped" adducts), [(**L1**)$_2$I]$^+$, and [(**L1**)$_2$(I_2)$_2$]$^{2+}$ were also carried out in the presence of CH_2Cl_2 and CH_3CN (optimized geometries in Tables S24–S31 in the SI), implicitly taken into account by means of the Polarizable Continuum Model (PCM) approach in its Integral Equation Formalism variant (IEF-PCM),[48] which describes the cavity of the solute within the Self-Consistent Reaction Field (SCRF) through a set of overlapping spheres. The nature of the energy minima at the optimized geometries were verified by a vibrational analysis, computed by determining the second derivatives of the energy with respect to the orthogonal Cartesian atomic coordinates and subsequently transforming to mass-weighted coordinates. The vibrational analysis also provided thermochemical data used to evaluate Zero-Point Energies (ZPEs) and investigate the enthalpy and free energy variations at 298 K for adduct formation reactions (see main text and Table S9 in the SI). In addition, the vibrational analysis was exploited to calculate harmonic frequencies of Raman-active modes (Table S9 in the SI). All Raman wavenumbers discussed above and summarized in Table S9 are unscaled. Natural Bonding Orbitals,[51] natural charges, and Wiberg[53] bond indices were calculated at the optimized geometries. A Second Order Perturbation Theory (SOPT) Analysis of Fock Matrix in NBO Basis was also carried out to investigate intramolecular donor–acceptor bonding interactions. The program GaussView 6.0[64] and

Molden 6.9[65] were used to analyze optimized geometries, KS-MOs and NBOs isosurfaces, natural charge distributions and to generate MEP maps on electron density surfaces.

Synthesis of $[L1I]_n(I)_n$ (II) and $[L1(\mu\text{-Se})](I)_2$ (III).

Method A: An equimolar mixture of **L1** (30.0 mg, 9.0×10^{-5} mol) and I_2 (22.8 mg, 9.0×10^{-5} mol) in MeCN (30 mL) was stirred at room temperature in air for 24 hours. An orange solution formed from which a few dark red blocks of [**L1**I]$_n$(I)$_n$ (**II**) and a few yellow tablet crystals of [**L1**(μ-Se)](I)$_2$ (**III**) formed by slow evaporation at room temperature in air. A whitish powder together with irregular colourless crystals of [**L1'**](I)$_2$ (**I**) also formed. The identity of the compounds corresponding to the three types of crystals could only be verified by X-ray diffraction analysis because of the very low isolable amount of each compound. **Method B**: An equimolar mixture of **L1** (60.0 mg, 1.8×10^{-4} mol), I_2 (45.69 mg, 1.8×10^{-4} mol) and Se powder (14.21 mg, 1.8×10^{-4} mol) in MeCN (30 mL) was stirred at room temperature in air for 72 hours. A yellowish solid formed, which was separated by filtration and washed with CH_2Cl_2. From the solution dark red blocks of [**L1**I]$_n$(I)$_n$ (**II**) formed by slow evaporation at room temperature in air (7.5 mg, 7.1% yield). Elemental analysis (%) calcd. for $C_9H_{12}I_2N_4Se_2$ (587.95): C 18.39, H 2.06, N 9.53; Found: C 18.41, H 2.03, N 9.55. M.p.: 193 ºC. ESI(+)-MS (MeCN solution) *m/z*: 463 ($[C_9H_{12}IN_4Se_2]^+$) 62%, 336 ($[C_9H_{12}N_4Se_2]^+$) 22%, 175 ($[C_5H_7N_2Se]^+$) 100%. $^{77}Se\{^1H\}$ (57,26 MHz, DMSO-d_6, 25 ºC): δ 162.08 ppm. FT-Raman in the range 500-65 cm^{-1} ν(I–I) (relative intensity): 183.5 (2), 133.5 (10), 94 (2). The yellowish solid separated from the reaction mixture proved to be composed of [**L1**(μ-Se)](I)$_2$ and unreacted Se powder. Unreacted Se powder was removed by decantation and the recovered yellow [**L1**(μ-Se)](I)$_2$ (54.4 mg, 45.3% yield) was washed with Et_2O. Elemental analysis (%) calcd. for $C_9H_{12}I_2N_4Se_3$ (666.91): C 16.21, H 1.81, N 8.40; Found: C 16.15, H 1.83, N 8.45. M.P. 221 ºC. ESI(+)-MS (MeCN solution) *m/z*: 644 ($[C_9H_{12}IN_4Se_3 + Se + Na]^+$) 33%, 541 ($[C_9H_{12}IN_4Se_3]^+$) 16%, 463 ($[C_9H_{12}IN_4Se_2]^+$) 76%, 336 ($[C_9H_{12}N_4Se_2]^+$) 32%. FT-Raman in the range 500-65 cm^{-1} ν(I–I) (relative intensity): 230 (10), 215 (6).

Synthesis of [L1I](I$_3$)·2I$_2$ (IV).

A mixture of **L1** (30.0 mg, 9.0×10^{-5} mol) and I_2 (91.4 mg, 1.8×10^{-4} mol) in MeCN (30 mL) was stirred at room temperature in air for 24 h. Dark red crystals corresponding to the formulation $C_9H_{12}I_8N_4Se_2$ (83.7 mg, 68.9% yield), formed from the reaction mixture by slow evaporation of the solvent in air. The crystals were isolated and washed with Et_2O. Elemental analysis (%) calcd. for $C_9H_{12}I_8N_4Se_2$ (1349.37): C 8.01, H 0.90, N 4.15; Found: C 7.98, H 0.95, N 4.10. M.p.: 120 ^oC. ESI(+)-MS (MeCN solution) *m/z*: 463 ($[C_9H_{12}IN_4Se_2]^+$) 9%. $^{77}Se\{^1H\}$ (57.26 MHz, DMSO-d_6, 25 ^oC): δ 343.31 ppm. FT-Raman in the range 500-65 cm^{-1} ν(I–I) (relative intensity): 101 (3.4), 145 (10), 170 (8), 186 (3,4).

Synthesis of [L2](I)$_2$·MeCN (V).

A mixture of **L2** (40.0 g, 1.15×10^{-4} mol) and I_2 (29.2 mg, 1.15×10^{-4} mol) in MeCN (30 mL) was stirred at room temperature for 24 hours in air. A yellow solid formed corresponding to the formulation $C_{12}H_{17}I_2N_5Se_2$ (*vide infra*), which was filtered and washed with Et_2O (46.1 mg, 62.4% yield). Yellow crystals of compound **V** were grown from a MeCN solution by slow evaporation in air. Elemental analysis (%) calcd. for $C_{12}H_{17}I_2N_5Se_2$ (643.026): C 22.41, H 2.66, N 10.89; Found: C 22.39, H 2.64, N 10.90. M.p.: 142 ^oC. ESI(+)-MS (MeCN solution) *m/z*: 476.8 ($[C_{10}H_{14}IN_4Se_2]^+$) 54%, 350 ($[C_{10}H_{14}N_4Se_2]^+$) 24%, 175 ($[C_5H_7SeN_2]^+$) 100%. $^{77}Se\{^1H\}$ (57.26 MHz, DMSO-d_6, 25 ^oC): δ 298.93 ppm. FT-Raman in the range 500-65 cm^{-1} ν(I–I) (relative intensity): 240 (10), 189 (1.3).[14a]

Synthesis of [L2](I$_3$·½I$_4$) (VI).

A mixture of **L2** (40.0 g, 1.15×10^{-4} mol) and I_2 (58.3 mg, 2.30×10^{-4} mol) in MeCN (30 mL) was stirred at room temperature for 24 hours in air. A first crop of dark red crystals corresponding to the

formulation of compound **VI** (30.8 mg, 27.3% yield) was obtained from the reaction mixture by partial slow evaporation of the solvent in air. These crystals were isolated and washed with Et_2O. Elemental analysis (%) calcd. for $C_{10}H_{14}I_5N_4Se_2$ (982.69): C 12.22, H 1.44, N 5.70; Found: C 12.26, H 1.40, N 5.75. M.p.: 206 °C. ESI(+)-MS (MeCN solution) *m/z*: 477 ($[C_{10}H_{14}IN_4Se_2]^+$) 31%, 350 ($[C_{10}H_{14}N_4Se_2]^+$) 8%, 175 ($[C_5H_7N_2Se]^+$) 51%. $^{77}Se\{^1H\}$ (57.26 MHz, DMSO-d_6, 25 °C): δ 341.36 ppm. FT-Raman in the range 500-65 cm^{-1} ν(I–I) (relative intensity): 227 (5.7), 189 (0.7), 155 (10), 141 (4.8), 112 (9.5).[14a] A second crop of dark red and yellow crystals corresponding to [**L2**]$(I)_2$·MeCN (**V**) and [**L2**]$(I_3 \cdot ½I_4)$ (**VI**), respectively (as verified by X-ray diffraction analysis), was obtained after further evaporation of the solution remaining from the first crystallization (22.1 mg overall). A mixture of crystals of **V** and **VI** (2.9 mg overall) was also obtained by cooling down a hot MeCN (10 mL) orange solution of **2** in Scheme 3 (13.0 mg, 1.5×10^{-5} mol).

Synthesis of [L2Se](I)$_2$.

A mixture of **L2** (60.0 mg, 1.72×10^{-4} mol), I_2 (43.7 mg, 1.72×10^{-4} mol) and Se powder (13.6 mg, 1.72×10^{-4} mol) CH_2Cl_2 (30 mL) was stirred at room temperature for 72 hours in air. The resulting greenish solid composed of compound [**L2**Se]$(I)_2$ and unreacted Se, was isolated and washed with CH_2Cl_2. Unreacted Se powder was removed by decantation and the recovered yellow compound [**L2**Se]$(I)_2$ (90.4 mg, 77.19% yield) was washed with Et_2O. Elemental analysis (%) calcd. for $C_{10}H_{14}I_2N_4Se_3$ (680.93): C 17.64, H 2.07, N 8.23; Found: C 17.61, H 2.04, N 8.20. M.P.: 156 °C. ESI(+)-MS (MeCN solution) *m/z*: 681 ($[C_{10}H_{14}I_2N_4Se_3\text{-}H]^+$) 8%. FT-Raman in the range 500-65 cm^{-1} ν(I–I) (relative intensity): 229 (10), 188 (1.7).

CONCLUSIONS

In this paper, we have reported the results achieved investigating the reactivity of bis-4-imidazoline-2-selone derivatives (RE) **L1** and **L2** towards I_2 in MeCN in comparison with those obtained from analogous reactions in CH_2Cl_2. The results described can allow to better

understand the main factors that influence the outcoming of such reactions, which are of pivotal importance in the understanding the biochemical processes at the base of the anti-thyroid drugs activity taking place in the thyroid peroxidase (TPO)/H_2O_2/I^- enzymatic system within the thyroid gland.[1-3, 8-15]

The variety of the products isolated and characterized (among them the first example of an iodonium complex with an imidazoline-2-selone derivative) clearly underline the importance of the experimental conditions, in particular the polarity of the solvent, as well as the nature of the reactants in determining the outcome of these kind of reactions. Furthermore, the results support the central role that the hypothetical intermediate $[RE–X]^+$ (R = organic framework, E = S, Se, X = halogen) cation or $[RE–X]^{\delta+}\cdots X^{\delta-}$ polarized species, hypothesized by Husebye, might have in the formation of the products isolated in the solid state, whose formation is favoured in more polar solvents (Figure 12).

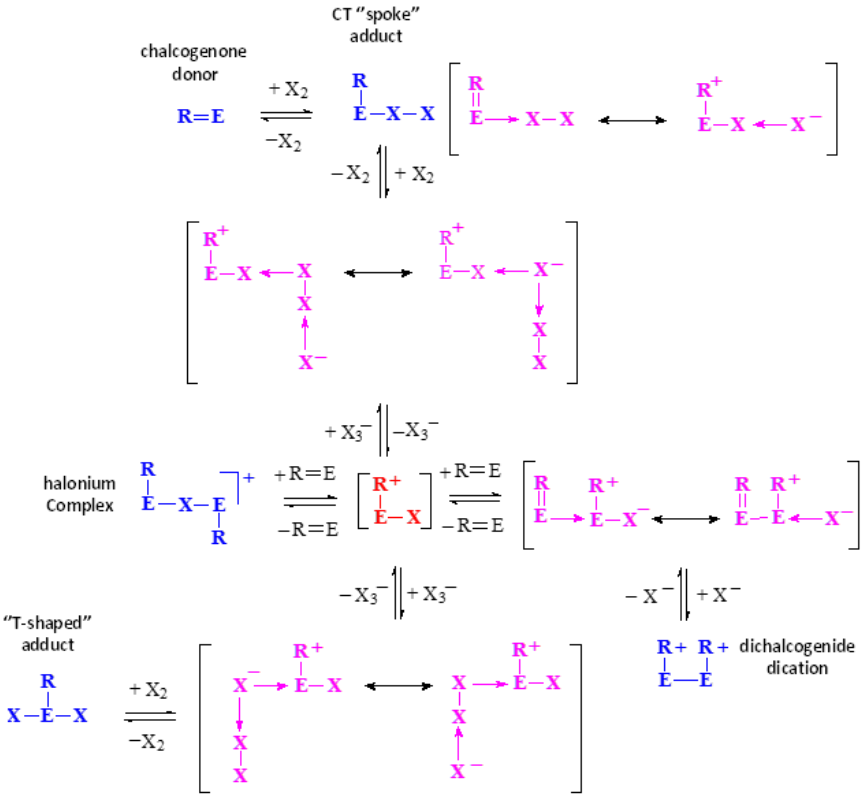

Figure 12. Possible reaction pathways to the formation of the known products isolated in the solid state from RE/X_2 reaction systems (RE chalcogenone donor; X_2 di-halogen molecule).

Interestingly, beside CT "spoke" and "T-shaped" adducts, halonium complexes and dichalcogenide cations (in blue in Figure 12), highly polarized CT "spoke" adducts and "extended spoke" CT adducts with different bond polarization pathways, dichalcogenide dications interacting with an halide ion and "T-shaped" adducts interacting with di-halogen molecules (in magenta in Figure 12) are all structural archetypes observed in the sold state depending on the nature and molecular structure of the RE chalcogenone donor, the di-halogen acceptor and the experimental conditions (reaction molar ratio and solvents). Regardless of its formation, the natural charge distribution calculated for the cation $[RE{-}X]^+$ at DFT level has proved to be of great help in making predictions of the possible final products in the solid state formed from RE/X_2 reaction systems. Polar solvents and, thus polarizing reaction conditions, will help in driving the reactions towards ionic or polarized products.

From a theoretical point of view, several further conclusions can be drawn from the results reported here. First, the combined use of the mPW1PW hybrid functional and LANL08 basis set with relativistic effective core potentials for halogens is confirmed as a very effective and affordable setup for halogen- and chalcogen-bonded neutral and charged systems, even when compared with the computationally more expensive M06-2X/aug-cc-PVTZ setup.

Many of the systems examined in this work show interactions that clearly fall in the realm of halogen- (HB) and chalcogen-bonds (ChB). For these systems, two apparently opposing interpretation models have been proposed to account for the interaction between a nucleophile and an electrophile synthon, *viz.* a MO-mixing approach, consisting of a partial electron density donation from a nucleophile (Lewis base) to an electrophile (Lewis acid), or an noncovalent σ-hole interpretation based on the topology of electrostatic potential. Many authors, by means of different decomposition schemes, have shown that both aspects contribute to XB and ChB interactions. In the limited selection of molecular and ionic systems dealt with here, it is clearly shown that the two models converge to the same conclusions, the depletion areas of electrostatic potential (σ-holes) being topologically related to the direction of antibonding natural orbitals.

ASSOCIATED CONTENT

Supporting Information (SI)

The Supporting Information is available free of charge at https://pubs.acs.org/doi/10.1021/acs.inorgchem.....

Supporting Figure S1, ESI(+) MS spectrum of [**L1**I]$_n$(I)$_n$ (**II**); Figure S2, ESI(+) MS spectrum of [**L1**(μ-Se)](I)$_2$ (**III**); Figure S3, Packing diagram of [**L1'**](I)$_2$ (**I**); Scheme S1, Examples from the literature of deselenation of cyclic pentatomic selones; Scheme S2, Product formed from the reaction of L2 with TCNQ; Figure S4, FT-Raman spectrum of compound [**L1**I]$_n$(I)$_n$ (**II**); Figure S5, View of the asymmetric unit in compound [**L1**(μ-Se)](I)$_2$·½H$_2$O (**III**) with disordered atoms; Figure S6, Se−I Interactions of the iodide ions in the asymmetric unit of [**L1**(μ-Se)](I)$_2$·½H$_2$O (**III**); Figure S7, FT-Raman spectrum of compound [**L1**(μ-Se)](I)$_2$·½H$_2$O (**III**); Figure S8, ESI(+) MS spectrum of [**L1**I](I$_3$)·2I$_2$ (**IV**); Figure S9, ESI(+) tandem MS spectrum of the peak at 463 *m/z* observed for [**L1**I](I$_3$)·2I$_2$ (**IV**); Figure S10, FT-Raman spectrum of compound [**L1**I](I$_3$)·2I$_2$ (**IV**); Figure S11, ESI(+) MS spectrum of [**L2**](I)$_2$·MeCN (**V**); Figure S12, ESI(+) tandem MS spectrum of the peak at 476.8 *m/z* observed for [**L2**](I)$_2$·MeCN (**V**); Figure S13, ESI(+) MS spectrum of [**L2**](I$_3$·½I$_4$) (**VI**); Figure S14, ESI(+) tandem MS spectrum of the peak at 477 *m/z* observed for [**L2**](I$_3$·½I$_4$) (**VI**); Figure S15, View of the structure of compound [**L2**](I)$_2$·MeCN (**V**) with disordered atoms; Figure S16, ESI(+) MS spectrum of [**L2**Se](I)$_2$; Figure S17, FT-Raman spectrum of compound [**L2**Se](I)$_2$; Figure S18, KS-HOMO calculated for **L1**; Figure S19, "T-shaped" and "spoke adducts" optimized for **L1**·2I$_2$; Figure S20, KS-LUMO calculated for [**L1**(I)$_2$]$^{2+}$; Figure S21, MEP map and KS-LUMO calculated for [**L1'**]$^{2+}$; Figure S22, MEP map calculated for [**L1**(μ-Se)]$^{2+}$; Figure S23, Antibonding NBOs calculated for [**L1**(μ -Se)]$^{2+}$; Figure S24, MEP map calculated for [**L2**]$^{2+}$; Figure S25, Antibonding NBOs calculated for [**L2**]$^{2+}$; Table S1, Crystal data and refinement parameters for compounds structurally characterized; Tables S2-S6, Selected bond lengths (Å) and angles (°) for compounds **I**-**V**; Table S7, Experimental and optimized selected metric parameters for "spoke" CT

and “T-shaped” adducts formed by **L1**/**L2** and I_2; Table S8, Selected metric parameters and natural charges calculated for the compounds optimized at DFT level; Table S9, Main Raman frequencies, total electronic energies, sum of electronic and zero-point energies, sum of electronic and thermal enthalpies, sum of electronic and thermal free energies calculated for the optimized compounds; Table S10-S35, Optimized geometry in orthogonal Cartesian coordinate format for the optimized compounds.

Accession Codes

CCDC: 2191254-2191258 contains the supplementary crystallographic data for this paper. These data can be obtained free of charge via www.ccdc.cam.ac.uk/data_request/cif, or by emailing data_request@ccdc.cam.ac.uk, or by contacting The Cambridge Crystallographic Data Centre, 12 Union Road, Cambridge CB2 1EZ, UK; fax: +44 1223 336033.

AUTHOR INFORMATION

Corresponding author

Vito Lippolis – Dipartimento di Scienze Chimiche e Geologiche, Università degli Studi di Cagliari, S.S. 554 Bivio per Sestu, 09042 Monserrato (CA), Italy; orcid.org/0000-0001-8093-576X; E-mail: lippolis**@**unica.it.

Authors

M. Carla Aragoni – Dipartimento di Scienze Chimiche e Geologiche, Università degli Studi di Cagliari, S.S. 554 Bivio per Sestu, 09042 Monserrato (CA), Italy; orcid.org/0000-0002-5010-7370.

Massimiliano Arca – Dipartimento di Scienze Chimiche e Geologiche, Università degli Studi di Cagliari, S.S. 554 Bivio per Sestu, 09042 Monserrato (CA), Italy; orcid.org/0000-0002-0058-6406.

Claudia Caltagirone – Dipartimento di Scienze Chimiche e Geologiche, Università degli Studi di Cagliari, S.S. 554 Bivio per Sestu, 09042 Monserrato (CA), Italy; orcid.org/0000-0002-4302-0234.

Carlo Castellano – Dipartimento di Chimica. Università degli Studi di Milano, Via Golgi 19, I-20133, Italy; orcid.org/0000-0002-7497-0670.

Francesco Demartin – Dipartimento di Chimica. Università degli Studi di Milano, Via Golgi 19, I-20133, Italy; orcid.org/0000-0003-2942-3990.

Peter G. Jones – Institut für Anorganische und Analytische Chemie der Technischen Universität Braunschweig. Hagenring 30, D-38106, Braunschweig, Geramny;

Tiziana Pivetta – Dipartimento di Scienze Chimiche e Geologiche, Università degli Studi di Cagliari, S.S. 554 Bivio per Sestu, 09042 Monserrato (CA), Italy; orcid.org/0000-0001-9881-3584.

Enrico Podda – Dipartimento di Scienze Chimiche e Geologiche and Centro Servizi di Ateneo per la Ricerca-CeSAR, Università degli Studi di Cagliari, S.S. 554 Bivio per Sestu, 09042 Monserrato (CA), Italy; orcid.org/0000-0002-4329-7751.

Sergio Murgia – Dipartimento di Scienze della Vita e dell'Ambiente, Università degli Studi di Cagliari, S.S. 554 Bivio per Sestu, 09042 Monserrato (CA), Italy; orcid.org/0000-0002-9986-0638.

Giacomo Picci – Dipartimento di Scienze Chimiche e Geologiche, Università degli Studi di Cagliari, S.S. 554 Bivio per Sestu, 09042 Monserrato (CA), Italy; orcid.org/0000-0002-3688-4464

Author Contributions

The manuscript was written through contributions of all authors. All authors have given approval to the final version of the manuscript.

Notes

The authors declare no competing financial interests.

ACKNOWLEDGMENTS

We thank Fondazione di Sardegna (FdS Progetti Biennali di Ateneo, annualità 2018 and 2020) for financial support, and CeSAR (Centro Servizi d'Ateneo per la Ricerca) of the University of Cagliari, for providing Raman and XRD facilities.

Keywords: Chalcogenone donors, 4-imidazoline-2-selone, di-iodine, triselane, iodonium complex, DFT calculations

Conflict of Interest

The authors declare no conflict of interest.

REFERENCES

(1) Roy, G.; Mugesh, G. Selenium analogues of anti-thyroid drugs. *Phosph., Silicon & Relat. Elem.* **2008**, *183*, 908-923.

(2) Manna, D.; Roy, G.; Mugesh, G. Antithyroid drugs and their analogues: Synthesis, structure, and mechanism of action. *Acc. Chem. Res.* **2013**, *46*, 2706-2715.

(3) Roy, G.; Jayaram, P. N.; Mugesh, G. Inhibition of lactoperoxidase-catalyzed oxidation by imidazole-based thiones and selones: A mechanistic study. *Chem. Asian J.* **2013**, *8*, 1910-1921.

(4) Rijntjes, E.; Scholz, P. M.; Mugesh, G.; Köhrle, J. Se- and S-Based Thiouracil and Methimazole Analogues Exert Different Inhibitory Mechanisms on Type 1 and Type 2 Deiodinases. *Eur. Thyroid j.* **2013**, *2*, 252-258.

(5) Battin, E. E.; Zimmerman, M. T.; Ramoutar, R. R.; Quarles, C. E.; Brumaghim, J. L. Preventing metal-mediated oxidative DNA damage with selenium compounds. *Metallomics* **2011**, *3*, 503-512.

(6) Zimmermann, M. T.; Bayse, C. A.; Ramoutar, R. R.; Brumaghin, J. L. Sulfur and selenium antioxidants: Challenging radical scavenging mechanisms and developing structure-activity relationships based on metal binding. *J. Inorg. Biochem.* **2015**, *145*, 30-40.

(7) Battin, E. E.; Brumaghim, J. L. Antioxidant Activity of Sulfur and Selenium: A review of reactive oxygen Species scavenging, glutathione peroxidase, and metal-binding antioxidant mechanisms. *Cell Biochem. Biophys.* **2009**, *55*, 1-23.

(8) (a) Kimani, M. M.; Wang, H. C.; Brumaghim, J. L. Investigating the copper coordination, electrochemistry, and Cu(II) reduction kinetics of biologically relevant selone and thione compounds. *Dalton Trans.* **2012**, *41*, 5248-5259; (b) Kimani, M. M.; Brumaghim, J. L.; Vanderveer, D. Probing the antioxidant action of selenium and sulfur using Cu(I)-chalcogenone tris(pyrazolyl)methane and-borate complexes. *Inorg. Chem.* **2010**, *49*, 9200-9211; (c) Roy, G.; Nethaji, M.; Mugesh, G. Bioinorganic chemistry of anti-thyroid

drugs: An unusual formation of a copper(II) complex. *Inorg. Chem. Commun.* **2006**, *9*, 571-574; (d) Kimani, M. M.; Watts, D.; Graham, L. A.; Rabinovich, D.; Yap, G. P. A.; Brumaghim, J. L. Dinuclear copper(I) complexes with N-heterocyclic thione and selone ligands: Synthesis, characterization, and electrochemical studies. *Dalton Trans.* **2015**, *44*, 16313-16324.

(9) (a) Davidson, B.; Soodak, M.; Neary, J. T.; Strout, H. V.; Kieffer, J. D.; Mover, H.; Maloof, F. The irreversible inactivation of thyroid peroxidase by methylmercaptoimidazole, thiouracil, and propylthiouracil in vitro and its relationship to in vivo findings. *Endocrynology* **1978**, *103*, 871-882; (b) Taurog, A.; Dorris, M. L.; Guziec Jr., F. S. Metabolism of 35s- and 14c-labeled l-methyl-2 mercaptoimidazole in vitro and in vivo. *Endocrynology* **1989**, *124*, 30-39.

(10) Basosi, R.; Niccolai, N.; Rossi, C. Coordination behaviour of antithyroid drugs against the $Fe(I)(NO)_2$ group in solution: ESR and FT-NMR study. *Biophys. Chem.* **1978**, *8*, 405069.

(11) Du Mont, W. W.; Mugesh, G.; Wismach, C.; Jones, P. G. Reactions of organoselenenyl iodides with thiouracil drugs: An enzyme mimetic study on the inhibition of iodothyronine deiodinase. *Angew. Chem., Int. Ed.* **2001**, *40*, 2486-2489.

(12) (a) Roy, G.; Mugesh, G. Anti-thyroid drugs and thyroid hormone synthesis: Effect of methimazole derivatives on peroxidase-catalyzed reactions. *J. Am. Chem. Soc.* **2005**, *127*, 15207-15217; (b) Bhabak, K. P.; Mugesh, G. Inhibition of peroxidase-catalyzed protein tyrosine nitration by antithyroid drugs and their analogues. *Inorg. Chim. Acta* **2010**, *363*, 2812-2818.

(13) (a) Isaia, F.; Aragoni, M. C.; Arca, M.; Demartin, F.; Devillanova, F. A.; Floris, G.; Garau, A.; Hursthouse, M. B.; Lippolis, V.; Medda, R.; Oppo, F.; Pira, M.; Verani, G. Interaction of methimazole with I_2: X-ray crystal structure of the charge transfer complex methimazole-I_2. Implications for the mechanism of action of methimazole-based antithyroid drugs. *J. Med. Chem.* **2008**, *51*, 4050-4053; (b) Aragoni, M. C.; Arca, M.; Demartin, F.; Devillanova, F. A.; Garau, A.; Isaia, F.; Lippolis, V.; Verani, G. Anti-Thyroid Drug Methimazole: X-ray Characterization of Two Novel Ionic Disulfides Obtained from Its Chemical Oxidation by I_2. *J. Am. Chem. Soc.* **2002**, *124*, 4358-4539; (c) Roy, G.; Nethaji, M.; Mugesh, G. Interaction of anti-thyroid drugs with iodine: the isolation of two unusual ionic compounds derived from Se-methimazole. *Org. Biomol. Chem.* **2006**, *4*, 2883-2887; (d) Freeman, F.; Ziller, J. W.; Po, H. N.; Keindl, M. C. Reactions of imidazole-2-thiones with molecular iodine and the structures of two

crystalline modifications of the 1:1 1,3-dimethylimidazole-2-thione-diiodine charge-transfer complex ($C_5H_8I_2N_2S$). *J. Am. Chem. Soc.* **1988**, *10*, 2586-2591.

(14) (a) Bigoli, F.; Demartin, F.; Deplano, P.; Devillanova, F. A.; Isaia, F.; Lippolis, V.; Mercuri, M. L.; Pellinghelli, M. A.; Trogu, E. F. Synthesis, Characterization, and Crystal Structures of New Dications Bearing the −Se−Se− Bridge. *Inorg. Chem.* **1996**, *35*, 3194-3201; (b) Bigoli, F.; Pellinghelli, A.; Deplano, P.; Devillanova, F.; Lippolis, V.; Mercuri, M.; Trogu, E. Reaction of Imidazole-2-selone Derivatives with Diiodine: Synthesis, Structural and Spectroscopic Characterization of the Adduct 1,1'-Bis (3-methyl-4-imidazolin-2-selone)methene bis(diiodine) and of the First Examples of I–Se–I Hypervalent Selenium-Compounds: 1,3-Dimethyl-4-imidazolin-2-ylium diiodo selenanide and 1,2-Bis (3-methyl-4-imidazolin-2-ylium diiodo selenanide)etane bis(dichlorometahne). *Gazz. Chim. Ital.* **1994**, *124*, 445-454; (c) Williams, D. J.; Vanderveer, D.; Crouse, B. R.; Raye, R. R.; Carter, T.; Hagen, K. S.; Brewer, M. Spectroscopic Properties and Molecular Structure of 1,3-Dimethyl-2-(Se,Se-dibromoseleno)-2(3H)-imidazolylidene. *Main Group Chem.* **1997**, *2*, 61-66.

(15) (a) Kuhn, N.; Fawzi, R.; Kratz, T.; Steimann, M.; Henkel, G. Zur Oxidation von 2-Selenoimidazolinen mit Iod[1]. *Phosph., Silicon & Relat. Elem.* **1996**, *112*, 225-233; (b) Aragoni, M. C.; Arca, M.; Blake, A. J.; Cadoni, E.; Copolovici, L. O.; Isaia, F.; Lippolis, V.; Murgia, S.; Pop, A. M.; Silvestru, C.; Tidey, J. P.; Varga, R. A. Reaction of imidazoline-2-selone derivatives with mesityltellurenyl iodide: a unique example of a 3c-4e Se→Te←Se three-body system embedding a tellurenyl cation. *New J. Chem.* **2019**, *43*, 11821-11831; (c) Aragoni, M. C.; Arca, M.; Demartin, F.; Devillanova, Francesco A.; Garau, A.; Grimaldi, P.; Isaia, F.; Lelj, F.; Lippolis, V.; Verani, G. First ICN Adduct with a Selenium Donor (R = Se): Is It an Ionic $[RSeCN]^+I^-$ or a "T-Shaped" R(I)SeCN Hypervalent Compound? *Eur. J. Inorg. Chem.* **2004**, 2363-2368.

(16) Aragoni, M. C.; Arca, M.; Devillanova, F. A.; Garau, A.; Isaia, F.; Lippolis, V.; Verani, G. Charge-transfer adducts between donors containing chalcogens (S and Se) and di-iodine: solution studies. *Coord. Chem. Rev.* **1999**, *184*, 271-290.

(17) Boyle, P. D.; Godfrey, S. M. The reactions of sulfur and selenium donor molecules with dihalogens and interhalogens. *Coord. Chem. Rev.* **2001**, *223*, 265-299.

(18) Aragoni, M. C.; Arca, M.; Demartin, F.; Devillanova, F. A.; Garau, A.; Isaia, F.; Lippolis, V.; Verani, G. C. T. complexes and related compounds between S and Se containing donors and I_2, Br_2, IBr and ICl. *Trends Inorg. Chem.* **1999**, *6*, 1-18.

(19) Corban, G. J.; Hadjikakou, S. K.; Hadjiliadis, N.; Kubicki, M.; Tiekink, E. R. T.; Butler, I. S.;

Drougas, E.; Kosmas, A. M. Synthesis, Structural Characterization, and Computational Studies of Novel Diiodine Adducts with the Heterocyclic Thioamides N-Methylbenzothiazole-2-thione and Benzimidazole-2-thione: Implications with the Mechanism of Action of Antithyroid Drugs. *Inorg. Chem.* **2005**, *44*, 8617-8627.

(20) Demartin, F.; Deplano, P.; Devillanova, F. A.; Isaia, F.; Lippolis, V.; Verani, G. Conductivity, FT-Raman spectra, and x-ray crystal structures of two novel $[D_2I]I_n$ (n = 3 and D = N-methylbenzothiazole-2(3H)-selone; n = 7 and D = N-methylbenzothiazole-2(3H)-thione) iodonium salts. First example of $I^{-}{\cdot}3I_2$ heptaiodide. *Inorg. Chem.* **1993**, *32*, 3694-3699.

(21) (a) Cristiani, F.; Demartin, F.; Devillanova, F. A.; Isaia, F.; Lippolis, V.; Verani, G. Charge-Transfer Complexes of N-Methylthiazolidine-2(3H)-selone (1) and N-Methylbenzothiazole-2(3H)-selone (2) with I_2 and IBr: Crystal Structures of $1{\cdot}I_2$, $1{\cdot}I_{1.25}Br_{0.75}$, $2{\cdot}2I_2$ and $2{\cdot}2IBr$. *Inorg. Chem.* **1994**, *33*, 6315-6324; (b) Aragoni, M. C.; Arca, M.; Demartin, F.; Devillanova, F. A.; Gelbrich, T.; Garau, A.; Hursthouse, M. B.; Isaia, F.; Lippolis, V. Charge-Transfer Adducts of N-Methylthiazolidine-2-thione with IBr and I_2: An Example of Polymorphism Featuring Interpenetrating Three-Dimensional Subcomponent Assemblies and Halogen···π···Halogen Weak Interactions. *Cryst. Growth Des.* **2007**, *7*, 1284-1290; (c) Manjare, S. T.; Yadav, S.; Singh, H. B.; Butcher, R. J. Redox Reaction between Main-Group Elements (Te, Sn, Bi) and N-Heterocyclic-Carbene-Derived Selenium Halides: A Facile Method for the Preparation of Monomeric Halides. *Eur. J. Inorg. Chem.* **2013**, 5344-5357; (d) Manjare, S. T.; Singh, H. B.; Butcher, R. J. Oxidation of Carbene-Derived Selenium Diiodide with Silver Tetrafluoroborate – Isolation of Iodonium Ion Complexes with Selones. *Eur. J. Inorg. Chem.* **2013**, 2161-2166.

(22) Daga, V.; Hadjikakou, S. K.; Hadjiliadis, N.; Kubicki, M.; dos Santos, J. H. Z. d.; Butler, I. S. Synthesis, Spectroscopic and Structural Characterization of Novel Diiodine Adducts with the Heterocyclic Thioamides, Thiazolidine-2-thione (tzdtH), Benzothiazole-2-thione (bztzdtH) and Benzimidazole-2-thione (bzimtH). *Eur. J. Inorg. Chem.* **2002**, *7*, 1718-1728.

(23) Demartin, F.; Devillanova, F. A.; Isaia, F.; Lippolis, V.; Verani, G. Reaction of N,N′-dimethylimidazolidine-2-selone (L) with I_2. Crystal structure of the mixed-valence $(L{\cdot}I_2)(L_2)^{2+}{\cdot}2I_3^{-}$ compound. *Inorg. Chim. Acta* **1997**, *255*, 203-205.

(24) Devillanova, F. A.; Deplano, P.; Isaia, F.; Lippolis, V.; Mercuri, M. L.; Piludu, S.; Verano, G.; Demartin, F. Crystal structure and vibrational characterization of the reaction products of N-methylthiazolidine-2(3H)-selone (1) and N-methylbenzothiazole-2(3H)-selone (2) with Br2. *Polyhedron* **1998**, *17*, 305-312.

(25) Aragoni, M. C.; Arca, M.; Demartin, F.; Devillanova, F. A.; Garau, A.; Isaia, F.; Lelj, F.;

Lippolis, V.; Verani, G. Mechanistic Aspects of the Reaction between Br_2 and Chalcogenone Donors (LE; E=S, Se): Competitive Formation of 10–E–3, T-Shaped 1:1 Molecular Adducts, Charge-Transfer Adducts, and $[(LE)_2]^{2+}$ Dications. *Chem. Eur. J.* **2001**, *7*, 3122-3133.

(26) Bigoli, F.; Deplano, P.; Devillanova, F. A.; Lippolis, V.; Mercuri, M. L.; Pellinghelli, M. A.; Trogu, E. F. A Spectro- and Conductometric Study of the Reaction of Imidazoline-2-selone Derivatives with Bromine − Crystal Structure of 1,2-Bis(3-methyl-4-imidazolin-2-ylium dibromoselenanide)ethane. *Eur. J. Inorg. Chem.* **1998**, *1*, 137-141.

(27) Aragoni, M. C.; Arca, M.; Blake, A. J.; Devillanova, F. A.; du Mont, W. W.; Garau, A.; Isaia, F.; Lippolis, V.; Verani, G.; Wilson, C. 1,2-Bis (3-methyl-imidazolin-2-ylium iodobromoselenanide) ethane: Oxidative Addition of IBr at the Se Atom of a >C= Se Group. *Angew. Chem. Int. Ed. Engl*. **2001**, *40*, 4359-4362.

(28) Juárez-Pérez, E. J.; Aragoni, M. C.; Arca, M.; Blake, A. J.; Devillanova, F. A.; Garau, A.; Isaia, F.; Lippolis, V.; Núñez, R.; Pintus, A.; Wilson, C. A Unique Case of Oxidative Addition of Interhalogens IX (X=Cl, Br) to Organodiselone Ligands: Nature of the Chemical Bonding in Asymmetric I–Se–X Polarised Hypervalent Systems. *Chem. A Eur. J.* **2011**, *17*, 11497-11514.

(29) Manjare, S. T.; Sharma, S.; Singh, H. B.; Butcher, R. J. Facile synthesis of benzimidazolin-2-chalcogenones: Nature of the carbon-chalcogen bond. *J. Organom. Chem.* **2012**, *717*, 61-74.

(30) Yadav, S.; Manjare, S. T.; Singh, H. B.; Butcher, R. J. Transition metal mediated formation of dicationic diselenides stabilised by N-heterocyclic carbenes: designed synthesis. *Dalton Trans.* **2016**, *45*, 12015-12027.

(31) Rudd, M. D.; Lindeman, S. V.; Husebye, S. Three-centre, four-electron bonding and structural characteristics of two-coordinate iodine(I) complexes with halogen and chalcogen ligands. Synthesis, spectroscopic characterization and X-ray structural studies of (Triiodo)[tris(dimethylamino)phosphaneselenide]iodine(I) and Bis{(triiodo)[tri(N-morpholyl)phosphaneselenide]-iodine(I)}/diiodine molecular complex. *Acta Chem. Scand.* **1997**, *51*, 689-708.

(32) Ho, P. C.; Wang, J. Z.; Meloni, F.; Vargas-Baca, I. Chalcogen bonding in materials chemistry. *Coord. Chem. Rev*. **2020**, *422*, article 213464.

(33) Bigoli, F.; Deplano, P.; Devillanova, F. A.; Girlando, A.; Lippolis, V.; Mercuri, M. L.; Pellinghelli, M. A.; Trogu, E. F. Reaction of 1,2-Bis(2-selenoxo-3-methyl-4-imidazolinyl)ethane (ebis) with TCNQ: Crystal Structure and Characterization of the Mixed-Valence Compound $[2(ebis)^{2+}\cdot ebis]\cdot 2[(TCNQ)_3^{2-}]$. *Inorg. Chem*. **1996**, *35*, 5403-5406.

(34) Bigoli, F.; Deplano, P.; A. Devillanova, F.; Girlando, A.; Lippolis, V.; Mercuri, M. l.;

Pellinghelli, M. a.; F. Trogu E., New semiconductors obtained by reaction of 4-imidazoline-2-selonederivatives with TCNQ. Characterization and X-ray structure of $(C_9H_{12}N_4Se)^{2+}(TCNQ)_3^{2-}$. *J. Mat. Chem.* **1998**, *8*, 1145-1150.

(35) du Mont, W.-W.; Bätcher, M.; Daniliuc, C.; Devillanova, F. A.; Druckenbrodt, C.; Jeske, J.; Jones, P. G.; Lippolis, V.; Ruthe, F.; Seppälä, E. Soft–Soft Interactions Involving Iodoselenophosphonium Cations: Supramolecular Structures of Iodine Adducts of Bulky Trialkylphosphane Selenides. *Eur. J. Inorg. Chem.* **2008**, 4562-4577.

(36) Konu, J.; Chivers, T.; Tuononen, H. M. Synthesis, Spectroscopic, and Structural Investigation of the Cyclic $[N(PR_2E)_2]^+$ Cations (E = Se, Te; R = iPr, Ph): the Effect of Anion and R-Group Exchange. *Inorg. Chem.* **2006**, *45*, 10678-10687.

(37) Karri, R.; Chalana, A.; Kumar, B.; Jayadev, S. K.; Roy, G. Exploiting the κ^2-Fashioned Coordination of $[Se_2]$-Donor Ligand L_3Se for Facile Hg−C Bond Cleavage of Mercury Alkyls and Cytoprotection against Methylmercury-Induced Toxicity. *Chem. Eur. J.* **2019**, *25*, 12810-12819.

(38) Burchell, C. J.; Kilian, P.; Slawin, A. M. Z.; Woollins, J. D.; Tersago, K.; Van Alsenoy, C.; Blockhuys, F. $E_2(CN)_2$ (E = S, Se) and Related Compounds. *Inorg. Chem.* **2006**, *45*, 710-716.

(39) W. Koch, M. C. A Holthausen, *Chemist's Guide to Density Functional Theory*, Wiley-VCH: Weinheim, 2nd Edition ed.; **2002**.

(40) Adamo, C.; Barone, V. Exchange functionals with improved long-range behavior and adiabatic connection methods without adjustable parameters: The mPW and mPW1PW models. *J. Chem. Phys.* **1998**, *108*, 664-675.

(41) (a) Wadt, W. R.; Hay, P. J. Ab initio effective core potentials for molecular calculations. Potentials for main group elements Na to Bi. *J. Chem. Phys.* **1985**, *82*, 284-298; (b) Check, C. E.; Faust, T. O.; Bailey, J. M.; Wright, B. J.; Gilbert, T. M.; Sunderlin, L. S. Addition of polarization and diffuse functions to the LANL2DZ basis set for p-block elements. *J. Phys. Chem. A* **2001**, *105*, 8111-8116; (c) Roy, L. E.; Hay, P. J.; Martin, R. L. Revised basis set for the LANL effective core potentials. *J. Chem. Theory Comput.* **2008**, *4*, 1029-1031.

(42) Weigend, F.; Ahlrichs, R. Balanced basis sets of split valence, triple zeta valence and quadruple zeta valence quality for H to Rn: Design and assessment of accuracy. *Phys. Chem. Chem. Phys.* **2005**, *7*, 3297-3305.

(43) (a) Aragoni, M. C.; Arca, M.; Devillanova, F. A.; Isaia, F.; Lippolis, V. Adducts of S/Se Donors with Dihalogens as a Source of Information for Categorizing the Halogen Bonding. *Cryst. Growth Des*. **2012**, ***12***, 2769-2779; (b) Aragoni, M. C.; Arca, M.; Demartin, F.; Devillanova, F. A.; Garau, A.; Isaia, F.; Lippolis, V.; Verani, G. DFT calculations, structural

and spectroscopic studies on the products formed between IBr and N,N′-dimethylbenzoimidazole-2(3H)-thione and -2(3H)-selone. *Dalton Trans*. **2005**, 2252-2258; (c) Mancini, A.; Aragoni, M. C.; Bricklebank, N.; Castellano, C.; Demartin, F.; Isaia, F.; Lippolis, V.; Pintus, A.; Arca, M. Formation of T-Shaped versus Charge-Transfer Molecular Adducts in the Reactions Between Bis(thiocarbonyl) Donors and Br_2 and I_2. *Chem. Asian J.* **2013**, *8*, 639-647.

(44) Zhao, Y.; Truhlar, D. G. The Mo6 suite of density functionals for main group thermochemistry, thermochemical kinetics, noncovalent interactions, excited states, and transition elements: two new functionals and systematic testing of four Mo6-class functionals and 12 other functionals. *Theor. Chem. Acc.* **2008**, *120*, 215-241.

(45) (a) Dunning Jr, T. H. Gaussian basis sets for use in correlated molecular calculations. I. The atoms boron through neon and hydrogen. J. Chem. Phys. **1989**, *90*, 1007-1023; (b) Kendall, R. A.; Dunning Jr, T. H.; Harrison, R. J. Electron affinities of the first-row atoms revisited. Systematic basis sets and wave functions. *J. Chem. Phys.* **1992**, *96*, 6796-6806; (c) Wilson, A. K.; Woon, D. E.; Peterson, K. A.; Dunning Jr, T. H. Gaussian basis sets for use in correlated molecular calculations. IX. The atoms gallium through krypton. *J. Chem. Phys.* **1999**, *110*, 7667-7676; (d) Peterson, K. A.; Figgen, D.; Goll, E.; Stoll, H.; Dolg, M. Systematically convergent basis sets with relativistic pseudopotentials. II. Small-core pseudopotentials and correlation consistent basis sets for the post-d group 16-18 elements. *J. Chem. Phys*. **2003**, *119*, 11113-11123.

(46) Bauzá, A.; Alkorta, I.; Frontera, A.; Elguero, J. On the Reliability of Pure and Hybrid DFT Methods for the Evaluation of Halogen, Chalcogen, and Pnicogen Bonds Involving Anionic and Neutral Electron Donors. *J. Chem. Theory Comput.* **2013**, ***9***, 5201-5210.

(47) Kolář, M. H.; Hobza, P. Computer Modeling of Halogen Bonds and Other σ-Hole Interactions. *Chem. Rev*. **2016**, *116*, 5155-5187.

(48) Tomasi, J.; Mennucci, B.; Cammi, R. Quantum Mechanical Continuum Solvation Models. *Chem. Rev.* **2005**, *105*, 2999-3094.

(49) Aragoni, M. C.; Arca, M.; Devillanova, F. A.; Grimaldi, P.; Isaia, F.; Lelj, F.; Lippolis, V. Kinetic and Thermodynamic Aspects of the CT and T-shaped Adduct Formation Between 1,3-Dimethylimidazoline-2-thione (or -2-selone) and Halogens. *Eur. J. Inorg. Chem*. **2006**, 2166-2174.

(50) Garau, A.; Aragoni, M. C.; Arca, M.; Caltagirone, C.; Demartin, F.; Isaia, F.; Lippolis, V.; Pivetta, T. A new assembly of diiodine molecules at the 1,3-dimethylimidazole-2-thione (Me_2ImS) template: crystal structure of $(Me_2IMS)_2{\cdot}(I_2)_5$. *New J. Chem.* **2022**, *46*, 6870-6877.

(51) Reed, A. E.; Weinstock, R. B.; Weinhold, F. Natural population analysis. *J. Chem. Phys*. **1985**, *83*, 735-746.

(52) Arca, M.; Ciancaleoni, G.; Pintus, A. "Computational Methods to Study Chalcogen Bond", in "Chalcogen Chemistry: fundamentals and applications", V. Lippolis, C. Santi, E. J. Lenardão, A. L. Braga eds., RSC publishing, UK, 2022, in the press, and references therein.

(53) Wiberg, K. B. Application of the pople-santry-segal CNDO method to the cyclopropylcarbinyl and cyclobutyl cation and to bicyclobutane. *Tetrahedron* **1968**, *24*, 1083-1096.

(54) Masuri, S.; Cadoni, E.; Cabiddu, M. G.; Isaia, F.; Demuru, M. G.; Moráň, L.; Buček, D.; Vaňhara, P.; Havel, J.; Pivetta, T. The firts copper(II) complex with 1,10-phenanthroline and salubrinal with interesting biochemical properties. *Metallomics* **2020**, *12*, 891–901.

(55) Strohalm, M.; Kavan, D.; Novák, P.; Volný, M.; Havlíček V. mMass 3: Cross-platform Software Environment for Precise Analysis of Mass Spectrometric Data. *Anal. Chem.* **2010**, *82*, 4648-4651.

(56) CrysAlisPRO, Oxford Diffraction /Agilent Technologies UK Ltd, Yarnton, England.

(57) G. M. Sheldrick, "SHELXS-97 and SHELXL-97, Program for Crystal Structure Solution and Refinement," University of Gottingen, Gottingen, **1997**.

(58) Sheldrick, G. M. SHELXT – Integrated space-group and crystal-structure determination. *Acta Crystallogr. Sect. A* **2015**, *71*, 3-8.

(59) Bruker (2015). APEX3 v2015.5-2. Bruker AXS Inc., Madison, Wisconsin, USA.

(60) Dolomanov, O. V.; Bourhis, L. J.; Gildea, R. J.; Howard, J. A. K.; Puschmann, H. OLEX2: a complete structure solution, refinement and analysis program. *J. Appl. Crystallogr.* **2009**, *42*, 339-341.

(61) Spek, A. L. PLATON SQUEEZE: a tool for the calculation of disordered solvent contribution to the calculated structure factors. *Acta Crystallogr. Sect. C* **2015**, *71*, 9-18.

(62) Gaussian 16, Revision C.01, Frisch, M. J.; Trucks, G. W.; Schlegel, H. B.; Scuseria, G. E.; Robb, M. A.; Cheeseman, J. R.; Scalmani, G.; Barone, V.; Petersson, G. A.; Nakatsuji, H.; Li, X.; Caricato, M.; Marenich, A. V.; Bloino, J.; Janesko, B. G.; Gomperts, R.; Mennucci, B.; Hratchian, H. P.; Ortiz, J. V.; Izmaylov, A. F.; Sonnenberg, J. L.; Williams-Young, D.; Ding, F.; Lipparini, F.; Egidi, F.; Goings, J.; Peng, B.; Petrone, A.; Henderson, T.; Ranasinghe, D.; Zakrzewski, V. G.; Gao, J.; Rega, N.; Zheng, G.; Liang, W.; Hada, M.; Ehara, M.; Toyota, K.; Fukuda, R.; Hasegawa, J.; Ishida, M.; Nakajima, T.; Honda, Y.; Kitao, O.; Nakai, H.; Vreven, T.; Throssell, K.; Montgomery Jr., J. A.; Peralta, J. E.; Ogliaro, F.; Bearpark, M. J.; Heyd, J. J.; Brothers, E. N.; Kudin, K. N.; Staroverov, V. N.; Keith, T. A.; Kobayashi, R.;

Normand, J.; Raghavachari, K.; Rendell, A. P.; Burant, J. C.; Iyengar, S. S.; Tomasi, J.; Cossi, M.; Millam, J. M.; Klene, M.; Adamo, C.; Cammi, R.; Ochterski, J. W.; Martin, R. L.; Morokuma, K.; Farkas, O.; Foresman, J. B.; Fox, D. J. Gaussian, Inc., Wallingford CT, **2016**.

(63) Pritchard, B. P.; Altarawy, D.; Didier, B.; Gibson, T. D.; Windus, T. L. New basis set exchange: An open, up-to-date resource for ACNP Full Text the molecular science community. *J. Chem. Inf. Model.* **2019**, *59*, 4814-4820.

(64) R. Dennington, T. A. Keith, J. M. Millam, GaussView, Version 6; Semichem Inc.: Shawnee Mission, KS, **2016**.

(65) Schaftenaar, G.; Noordik, J. Molden: a pre- and post-processing program for molecular and electronic structures. *J. Comput. Aided Mol. Des.* **2000**, *14*, 123-134.

Graphycal Abstract

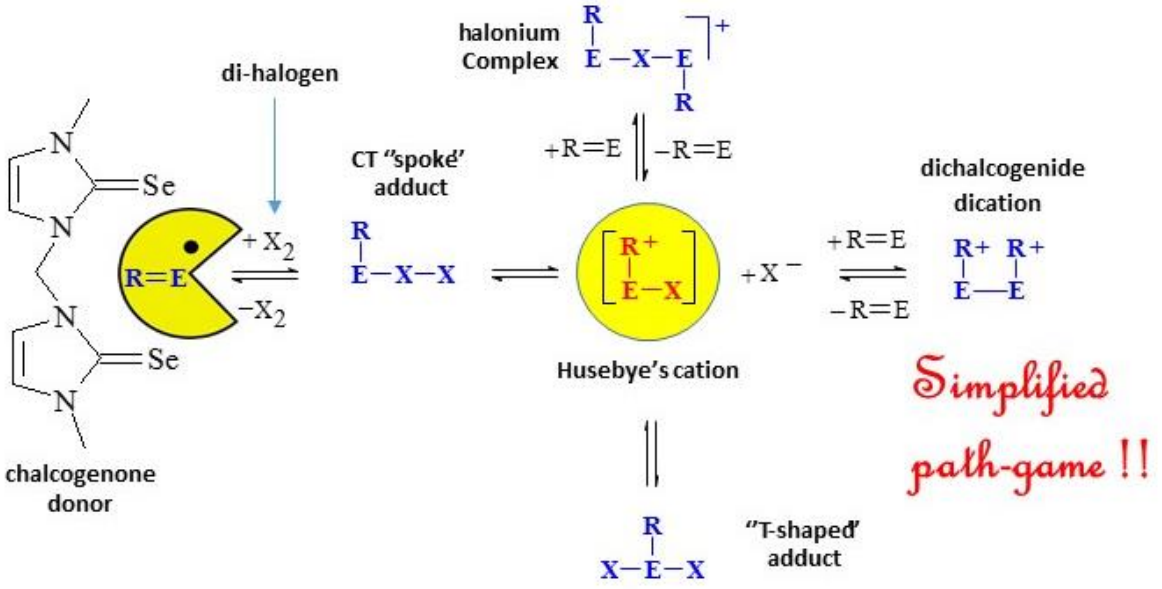

The reactivity of bis-4-imidazoline-2-selone derivatives (RE) towards I_2 in MeCN supports the formation of $[RE{-}X]^+$ cation intermediate in the reaction between chalcogenone donors and di-halogens and interhalogens with possible implication in the mechanism of action of anti-thyroid drugs.